Astrocyte-secreted C3 signaling impairs neuronal development and cognition in autoimmune diseases

Fan Zhu, Pengyan He, Wei Jiang, Shabbir Khan Afridi, Huiming Xu, Maali Alahmad, Yu-Wen Alvin Huang, Wei Qiu, Guangyou Wang, Changyong Tang

PII: S0301-0082(24)00090-X

DOI: https://doi.org/10.1016/j.pneurobio.2024.102654

Reference: PRONEU102654

To appear in: *Progress in Neurobiology*

Please cite this article as: Fan Zhu, Pengyan He, Wei Jiang, Shabbir Khan Afridi, Huiming Xu, Maali Alahmad, Yu-Wen Alvin Huang, Wei Qiu, Guangyou Wang and Changyong Tang, Astrocyte-secreted C3 signaling impairs neuronal development and cognition in autoimmune diseases, *Progress in Neurobiology,* (2024) doi:https://doi.org/10.1016/j.pneurobio.2024.102654

Astrocyte-secreted C3 signaling impairs neuronal development and cognition in autoimmune diseases

Fan Zhu[1]†, Pengyan He[1]†, Wei Jiang[1]†, Shabbir Khan Afridi[2], HuimingXu[1], Maali Alahmad[3], Yu-Wen Alvin Huang[4], Wei Qiu[1], Guangyou Wang[5]*, Changyong Tang[1]*

[1]Department of Neurology, The Third Affiliated Hospital of Sun Yat-Sen University; 600 Tianhe Road, Guangzhou 510630, Guangdong Province, China

[2]State Key Laboratory for Molecular and Developmental Biology, Institute of Genetics and Developmental Biology, Chinese Academy of Sciences, Beijing 100101, China Graduate School, University of Chinese Academy of Sciences, Beijing, China

[3]Faculty of Biological Sciences, School of Biomedical Sciences, University of Leeds, Leeds LS2 9JT, UK

[4]Department of Molecular Biology, Cell Biology, and Biochemistry, Brown University; 70 Ship Street, Providence, RI 02903

[5]Department of Neurology, First Affiliated Clinical Hospital of Harbin Medical University, and Department of Neurobiology, Harbin Medical University, Harbin 150081, China

*Corresponding authors. Email: tangchy23@mail.sysu.edu.cn (CT); wangguangyou@hrbmu.edu.cn (GW)

Author contributions

Conceptualization, C.T.; methodology, F.Z., W.J., and P.H.; investigation, F.Z., W.J., and P.H.; writing–original draft, C.T., A.S.K., F.Z., and W.J.; writing–review & editing, C.T., and A.S.K.; funding acquisition, C.T. supervision, C.T., G.W., W.Q; project administration, C.T.

Funding

This research was supported by grants from the National Natural Science Foundation of China (32100787), the Science and Technology Plan Project of Guangzhou City (202201020489 and 2023A04J1089), the National Natural Science Foundation of China

(32071036), Natural Science Foundation of Heilongjiang Province of China (ZD2022H001).

Acknowledgments

We thank Dr. Yaxiong Cui for helpful discussion and technical assistance.

Declaration of Interests

The authors declare no competing interests.

Abstract

Neuromyelitis optica (NMO) arises from primary astrocytopathy induced by autoantibodies targeting the astroglial protein aquaporin 4 (AQP4), leading to severe neurological sequelae such as vision loss, motor deficits, and cognitive decline. Mounting evidence has shown that dysregulated activation of complement components contributes to NMO pathogenesis. Complement C3 deficiency has been shown to protect against hippocampal neurodegeneration and cognitive decline in neurodegenerative disorders (e.g., Alzheimer's disease, AD) and autoimmune diseases (e.g., multiple sclerosis, MS). However, whether inhibiting the C3 signaling can ameliorate cognitive dysfunctions in NMO remains unclear. In this study, we found that the levels of C3a, a split product of C3, significantly correlate with cognitive impairment in our patient cohort. In response to the stimulation of AQP4 autoantibodies, astrocytes were activated to secrete complement C3, which inhibited the development of cultured neuronal dendritic arborization. NMO mouse models exhibited reduced adult hippocampal newborn neuronal dendritic and spine development, as well as impaired learning and memory functions, which could be rescued by decreasing C3 levels in astrocytes. Mechanistically, we found that C3a engaged with C3aR to impair neuronal development by dampening β-catenin signalling. Additionally, inhibition of the C3-C3aR-GSK3β/β-catenin cascade restored neuronal development and ameliorated cognitive impairments. Collectively, our results suggest a pivotal role of the activation of the C3-C3aR network in neuronal development and cognition through mediating astrocyte and adult-born neuron communication, which represents a potential therapeutic target for autoimmune-related cognitive impairment diseases.

Keywords:

Neuromyelitis optica; Cognitive impairments; C3 signaling; Astroctye

Introduction

The complement system plays a vital role in regulating immune responses, detecting and eliminating pathogens, as well as in the processes of development, regeneration, and maintaining tissue homeostasis (Holers, 2014; Mastellos *et al.*, 2023; Reis *et al.*, 2019). However, as a critical part at the early stage of inflammatory response, insufficient, excessive

or unregulated complement activation can result in a variety of human diseases varying in severity, location, and duration (Ricklin and Lambris, 2013; Ricklin *et al.*, 2016; Vignesh *et al.*, 2017; Wu *et al.*, 2019). The activation of the full complement system requires the coordinated actions of more than 30 proteins across three different pathways: classical, alternative, and mannose-binding lectin (Lian *et al.*, 2015a). The activation of the classical pathway involves the cleavage of the central complement factor C3 into C3a and C3b, which then trigger subsequent reactions by binding to their specific receptors, C3aR and CR3, respectively (Litvinchuk *et al.*, 2018; Stephan *et al.*, 2012). In disorders of the central nervous system, multiple complement proteins, receptors, and regulators are upregulated. According to previous studies, analyses of cerebrospinal fluid (CSF), blood, and post-mortem samples have showed a disturbance of the complement pathway in central nervous system disorders such as neuroinflammatory diseases (e.g., neuromyelitis optica, NMO and multiple sclerosis, MS), and neurodegenerative conditions (e.g., Alzheimer's disease, AD). Research has shown that the unique complement-specific drug, eculizumab, can block downstream processes when it targets C5 activation (Pittock *et al.*, 2019). Blocking C5 has not only allowed for more effective treatment for diseases with complement-mediated pathophysiology but has also uncovered new pathogenic mechanisms in conditions that are not responsive to the current anti-complement therapies. As C3 is located at the convergence of all three complement activation pathways, it is a perfect target for complement regulation. Efforts to develop therapies based on C3 have been initiated due to its crucial role in coordinating communication between various immune and inflammatory systems (Asavapanumas *et al.*, 2021; Xu *et al.*, 2023). Increasing evidence has indicated that C3-targeted interventions are potential therapeutic strategies that can be an alternative for the existing therapies (Asavapanumas *et al.*, 2021; Xu *et al.*, 2023).

NMO is a disease characterized by recurring attacks caused by antibodies in the central nervous system (CNS), primarily impacting the optic nerves, brain, and spinal cord. Serum autoantibodies specific for aquaporin 4 (AQP4) have been identified to be a typical pathological characteristic of NMO, unifying a spectrum of CNS demyelinating disorders and distinguishing them from multiple sclerosis (MS) (Lennon *et al.*, 2004). NMO with AQP4-IgG positivity is a clearly defined disease affecting astrocytes, characterized by the accumulation of immunoglobulin around blood vessels, activation of complement proteins, loss of myelin and axons, resulting in severe impairment of spinal cord and optic nerve functions, along with notable cognitive decline that significantly aggravates the disease burden (Asavapanumas *et al.*, 2021; Czarnecka *et al.*, 2020; Lopez-Soley *et al.*, 2022). There is ample evidence indicating that complement activation plays a key role in the pathogenesis following AQP4-IgG binding to AQP4, resulting in inflammation and demyelination (Asavapanumas *et al.*, 2021; Walker-Caulfield *et al.*, 2015). Both our group and other studies have discovered a notable increase in C3 levels in astrocytes when exposed to hsAQP4-IgG, both *in vitro* and *in vivo* (Chen *et al.*, 2020; Xu *et al.*, 2023). Moreover, individuals with NMO exhibit significantly increased levels of C3a, a split product of C3, which is closely linked to clinical disability measures (Expanded Disability Status Scale, EDSS) (Abboud *et al.*, 2022; Xu *et al.*, 2023).

Studies have shown that both anatomical and functional abnormalities in the hippocampus have been observed in NMO patients (Jiang *et al.*, 2023; Liu *et al.*, 2015; Zakani *et al.*, 2023), supporting the idea that hippocampal dysfunction is related to complement activation. Given the significant correlation between complement C3 levels and clinical severity in NMO (Nytrova *et al.*, 2014; Xu *et al.*, 2023), we are prompted to explore the role of C3 in the

progression of hippocampal dysfunction and cognitive decline in NMO animal models. Adult hippocampal newborn neurons arise from the division of stem and progenitor cells, a process known as adult neurogenesis (Cope and Gould, 2019). Neuronal maturation is a crucial stage in neurogenesis in both the embryonic and mature brain. Newborn dentate granule cells become part of the hippocampal neuronal circuitry through a series of stereotypic processes which consist of neuronal morphogenesis, migration, growth of axons and dendrites, and synapse formation (Denoth-Lippuner and Jessberger, 2021; Gonçalves *et al.*, 2016). It is believed that the interruption of dendritic growth in newly formed neurons in adults may play a role in the cognitive and emotional impairments seen in neurodegenerative and neuroimmune conditions (Llorens-Martín *et al.*, 2015; Sun *et al.*, 2009; Trinchero *et al.*, 2017; Zhang *et al.*, 2020). Based on our previous research on the development of newborn neurons and the signalling pathways of complement C3, we decided to focus on the development of newborn neurons in adults and aimed to delineate a cellular signalling pathway of C3 as a proof-of-concept for the functions of C3 in the brain.

In this study, we aimed to determine the signaling pathway by which C3 controls the negative impact on neuronal development by identifying the receptor and downstream pathway in newborn neurons. We initially validated that the levels of C3a, a split product of C3, were significantly elevated in individuals diagnosed with NMO and strongly correlated with cognitive function assessments. Remarkably, C3 released by hsAQP4-IgG-activated astrocytes significantly inhibited the dendritic development in cultured hippocampal primary neurons *in vitro*. For *in vivo* tests, we analyzed hippocampal tissues from young adult mice with C3 overexpression or passive transfer of anti-AQP4 IgG, which resulted in astrocyte activation and subsequent C3 secretion. We observed an evident reduction in the development of newborn neuron dendrites in the adult hippocampus and impaired cognitive abilities. Notably, neuronal development defects could be rescued by C3 knockdown in astrocytes. Mechanistically, C3 binds to its receptor C3aR and inhibits β-catenin signalling, which is essential for neurogenesis. Ultimately, we demonstrated that targeting the C3/C3aR/β-catenin pathway restored neuronal development and alleviated cognitive impairments caused by immune activation. This study provides brand-new evidence for the effect of C3 on neuronal development and cognitive functions in the NMO mouse model, apart from its traditional role as merely a component of innate immunity. These findings offered insights into the potential therapeutics to prevent cognitive dysfunction beyond NMO and other autoimmune brain diseases.

Results

The secretion of C3 is correlated to cognitive impairments and dysfunction in the hippocampus of human brains affected by autoimmune-induced astrocyte activation.

Our previous research confirmed that by stimulation of human anti-AQP4 autoantibodies (hsAQP4-IgG) purified from NMO patients' plasma, astrocytes were activated and secreted numerous inflammatory factors, such as complement C3, CCL2, 5, 6, 7, 17, CXCL1 and 10, as well as IL-1- α And IL-1- β, indicating the proinflammatory feature of hsAQP4-IgG (Fig. S1A and 1B) (Jiang *et al.*, 2023; Xu *et al.*, 2023). Our group and other previous research have shown that inhibiting C3 signalling can mitigate motor and visual impairments in an NMO mouse model (Chen *et al.*, 2020; Xu *et al.*, 2023). In addition, inhibiting C3 signalling also protects against hippocampal neurodegeneration and cognitive decline in aged AD mice despite the presence of abundant Aβ plaques (Shi *et al.*, 2017) and in experimental autoimmune encephalomyelitis (EAE), the animal model for multiple sclerosis (Bourel *et al.*, 2021).

To further investigate the clinical correlation between C3a levels and neuropsychological functions in a neuroinflammatory state, we analysed a cohort comprising 90 NMO patients with complete disease records and 80 age-matched healthy controls, whose sample size is larger than any other previous clinical case study (Table S1). Consistent with prior research (Jiang *et al.*, 2023; Nytrova *et al.*, 2014; Xu *et al.*, 2023), all patients had autoantibodies against AQP4 and the demographic information showed a predominant percentage of young women in the patients (average age 42.9±11.9 years; male/female ratio=7/83). We nest measured the levels of C3a in the serum and CSF of healthy controls and NMO patients and observed that the levels of C3 of NMO patients were significantly increased compared to healthy individuals (Fig. 1A, Table S1).

Specifically, we used neuropsychological assessment scales, including the Hamilton Anxiety Rating Scale (HARS) and Hamilton Depression Rating Scale (HDRS) for general anxiety and depression-like symptoms, as well as standard tests such as Mini Mental State Examination (MMSE), Symbol Digit Pattern Test (SDMT), and Short Visual Spatial Memory Revision Test (BVMT-R) (Fig. S1C) to assess neuropsychological functions of NMO patients and healthy individuals. In all assessments, we observed significant differences between the healthy controls and NMO patients (Fig. S1C), indicating that NMO patients have cognitive impairments in addition to focal neurological signs of motor and visual loss. Remarkably, neuropsychological impairments were strongly correlated with the levels of serum C3a in patients with NMO. Scores of HARS and HDRS were positively correlated with C3a levels, suggesting increased mental stress reactions due to disease burden (Fig. 1B and 1C, Fig. S1C). We were particularly struck by the potent negative correlation between C3a levels and the ability of learning and memorizing measured by MMSE, SDMT, and BVMT-R (Fig. 1D-1F). To figure out the structural basis of cognitive dysfunctions related to C3 expression in NMO, we conducted detailed analysis of hippocampal regions utilizing data based on MRI scans. Consistent with literature and our previous research (Cacciaguerra *et al.*, 2021; Jiang *et al.*, 2023; Liu *et al.*, 2015), our new NMO patient cohort exhibited noticeable hippocampal volume atrophy (Fig. S1D-1F), which was recognized as a structural basis for the cognitive impairment. Altogether, these findings suggest that C3 may be involved in hippocampal structural changes and mediating cognitive impairments in neuroimmune diseases.

Astrocyte-secreted C3 reduces neuronal development in immune-mediated

neuroinflammation.

Recent research showed that inhibiting the activity of C3 is sufficient to prevent early dendritic loss in the dentate gyrus of the hippocampus and memory impairment in EAE mice (Bourel *et al.*, 2021). C3 activation is related to the pathogenesis of NMO and may serve as an effective disease biomarker (Nytrova *et al.*, 2014). To verify our hypothesis that C3 released by activated astrocytes leads to hippocampal dysfunction and neuroinflammation-related cognitive impairment, we focused on a specific hippocampal cell type: adult-born hippocampal neurons. These neurons are crucial for maintaining the proper size and function of hippocampus and are extremely sensitive to a microenvironment with inflammation. Thus, to explore the effect of C3 on the hippocampal newborn neuron's development, we prepared high-purity (>95%) mouse hippocampal neurons (Fig. S1G) and treated them with C3 recombinant protein (100 ng/mL) or vehicle for 3 days (Fig. 1G). Compared with the vehicle group, the dendritic complexity of neurons treated with C3 recombinant protein was reduced (Fig. 1H). Furthermore, we also stimulated hippocampal primary neurons with 1, 10, 50 and 100 ng/mL of C3 protein for 3 days to observe the effects of different C3 concentrations on dendritic development of primary neurons (Figure S1L). The results showed that different concentrations of C3 recombinant protein significantly inhibited the development of primary neurons cultured for 7 days in a dose-dependent manner (Figure S1L). Next, we investigated whether the inhibitory effect of C3 recombinant protein on newborn neurons could also be observed in mature neurons cultured for 14 days. We found that mature neurons cultured for 14 days were able to resist the detrimental effects of different concentrations of C3 recombinant protein (Figure S1K). Given our previous findings that numerous inflammatory factors can be secreted by astrocytes activated by hsAQP4-IgG (Fig. S1A and 1B), we tested the effects of six other identified factors secreted by activated astrocytes on primary newborn neuronal dendritic development, including VCAM1, CXCL1, GBP5, IL1α, IL1β and ISG15. Strikingly, these inflammatory factors either did not affect dendritic development or exerted less influence on neurons than C3, suggesting that C3 was the core factor that inhibited the dendritic development of primary neurons in vitro (Fig. S1I). We also increased the concentration of the aforementioned 7 secreted proteins to 200 ng/mL to observe the effects of high concentration on the development of primary neurons. Our results showed that even in this situation, C3 remained to be the main protein that continuously affected neuronal development (Fig. S1J).

Furthermore, to directly investigate the effect of C3 released by activated astrocytes on neuronal dendritic arborization development, primary mouse astrocytes were treated with hsAQP4-IgG (100 ng/mL), or hsCtrl-IgG and the cultured supernatant was collected 24 hours after the IgG treatment, which we later named as astrocyte conditioned medium (ACM) (Fig. 1I). ELISA analysis showed that compared with astrocytes treated with hsCtrl-IgG, the levels of C3, C3a and C3b in the ACM of astrocytes stimulated with hsAQP4-IgG were significantly increased (Fig. 1J). To ascertain the necessity of C3, we removed it using a monoclonal neutralizing antibody targeting C3—an approach that effectively block the function of secreted C3 by astrocytes (Fig. 1I). By ELISA analysis, we proved that C3 neutralizing antibodies can effectively remove C3, C3a and C3b protein from ACM (Fig. 1J). As anticipated, ACM of astrocytes treated with hsAQP4-IgG impaired primary neuronal dendritic development (Fig. 1K). Besides, the application of the C3 neutralizing antibody reversed the inhibitory impact of the hsAQP4-IgG-ACM on neuronal dendritic development (Fig. 1L). In addition, we found that neuronal dendritic development was not inhibited with direct hsAQP4-IgG treatment in vitro (Fig, S1H). Taken together, these data showed that hsAQP4-

IgG impairs neuronal development by astrocytes-secreted C3 protein.

Immune-mediated astrocytopathy impairs the development of adult-born hippocampal neurons and hippocampus-dependent learning behaviours in young adult mice.

After demonstrating that C3 protein secreted by activated astrocytes reduces primary neuronal dendrites length and complexity in vitro (Fig. 1H), we then investigated whether this effect could be observed in an NMO mouse model. We employed a passive transfer strategy to construct a mouse model of immune-mediated astrocytopathy similar to NMO, by utilizing anti-AQP4 antibody (hsAQP4-IgG) or negative control antibody (hsCtrl-IgG). We stereotaxically injected a mixture of these antibodies and retrovirus expressing red fluorescent protein (RFP) to label newborn neurons into the bilateral dentate gyrus of 8-week-old mice (Fig.2A and 2B). Four weeks post-stereotaxic IgG delivery, we observed that, in comparison to the hsCtrl-IgG group, the hsAQP4-IgG-treated group displayed a decreased end-feet coverage along the micro-vessels of$AQP4^+$ astrocyte, which was identified as a classical NMO diagnostic feature (Fig. 2C). We also observed significant activation of microglia near the hippocampus four weeks after hsAQP4-IgG injection (FIG. S2A). Besides, the hsAQP4-IgG-treated group exhibited a lower fluorescence intensity of the tight junction protein ZO-1, revealing an increase in blood-brain barrier permeability (Fig. S2C). Surprisingly, the immune inflammatory response mediated by hsAQP4-IgG had no effect on the number of neurons ($NeuN^+$) (Fig. S2B) or the infiltration of $CD4^+$ or $CD8^+$ immune cells (Fig.S2D and 2E). In alignment with prior results, astrocytes in the hsAQP4-IgG group showed a significant increase in the expression level of GFAP and C3 (Fig. 2D).

To investigate the potential link between immune-mediated neuroinflammation and changes in adult-born neuronal development, we examined the dendritic morphology of newborn neurons four weeks after antibody injections (Fig. 2B). We found that passive injection of hsAQP4-IgG resulted in shorter dendrites and reduced dendritic complexity of RFP^+ newborn neurons in the hippocampal dentate gyrus (Fig. 2E), and a significant decreased density of dendritic spines (Fig. 2F). We hypothesized that these impairments in dendrite and dendritic spine development would exert a negative impact on neuronal activities and their integration with the hippocampal circuit. Moreover, compared to the control group, mice treated with hsAQP4-IgG had a significantly lower percentage of c-Fos-positive newly generated neurons ($BrdU^+NeuN^+$) (Fig. 2H), suggesting that these neurons were less active in the DG. These data reflect an impaired process of neuronal development triggered by immune-mediated neuroinflammation.

To assess the impact of astrocyte activation on cognitive function, a series of behavioral tests were conducted in NMO mouse model (Fig. 2G). Four to six weeks after the stereotaxic IgG transfer, mice were subjected to standardized behavioral assays, including the open field test (OFT), novel object location (NOL) test, novel object recognition (NOR) test, Morris water maze (MWM) task, and the reversal Morris water maze (RMWM) task as described in our previous research. The hsAQP4-IgG group of mice travelled shorter total distances and spent less time in the central area during the OFT (Fig. S2F), indicative of reduced locomotor activity and increased low curiosity-like behaviour. The hsAQP4-IgG group also exhibited deficits in spatial memory during the NOL test (Fig. S2G) and the NOR test (Fig. S2H). During the MWM task, mice treated with hsAQP4-IgG spent more time to locate the hidden platform (Fig. 2I). While in the probe test (the platform was removed during testing), hsAQP4-IgG treated mice spent less time in the target quadrant (Fig. S2I) and displayed fewer target quadrant crossings (Fig.2I), indicating that their spatial learning ability was compromised. In

the RMWM task, the hsAQP4-IgG group took significantly longer time to find the newly located platform (Fig. 2J) and crossed it for fewer times (Fig. 2J). They also spent less time in the target quadrant (Fig. S2J), indicating impaired spatial reversal learning and executive functions. Notably, we noticed no difference in the swimming ability between the two groups (Fig. S2I and 2J). These behavioural observations, along with the immunofluorescent data of histopathology, confirm that our astrocytopathy mouse model induced by hsAQP4-IgG represents important features of NMO pathology.

Additionally, we utilized mini-osmotic pump implantation to establish another passive transfer mouse model. In this experiment, retrovirus expressing red fluorescent protein (RFP) was first stereotaxically injected into the DG area to label newborn neurons. One week after the injection, a mini-osmotic pump containing hsCtrl-IgG or hsAQP4-IgG was implanted into the hippocampal regions of 8-week-old mice to enable continuous administration of the antibodies for two weeks. Four weeks after injection of retrovirus, we evaluated neuronal dendritic morphology (Fig. 2K). The infusion of hsAQP4-IgG led to a decline in dendritic length and complexity (Fig. 2L) and spine density (Fig. 2M) compared to hsCtrl-IgG control conditions.

Finally, we constructed a systemic NMOSD mouse model via intraperitoneal (I.P.) injection of hsCtrl-IgG, as described in our previous studies (Fig. S3A) (Yick *et al.*, 2020). Using a similar strategy to label newborn neurons by retrovirus, we observed that RFP^+ newborn neurons of the hsAQP4-IgG group exhibited shorter dendrites and lower complexity (Fig. S3B) and reduced spine density (Fig. S3C) in the hippocampus compared to the hsCtrl-IgG group. A battery of behavioral tests revealed similar cognitive deficits in the systemic NMOSD mouse model (Fig. S3D-3G). These results further confirmed that these different approaches—stereotaxic injection, chronic perfusion, and i.p. injection—yielded congruent outcomes, indicating that immune-mediated astrocytes activation inhibits the adult-born hippocampal neuronal development, which is potentially regulated by secreted C3 in a paracrine manner.

C3 is sufficient to hinder the development of neurons and impair hippocampal-dependent learning behaviours in young adult mice.

After demonstrating the inhibitory effects of C3 on primary neuronal dendritic development *in vitro* (Fig. 1H), we proceeded to explore whether similar outcomes could be observed *in vivo*. One week after administering retroviruses, we employed a minipump method to continuously infuse C3 into the dentate gyrus (DG) for two weeks (Fig. 3A). Compared to control groups, C3 infusion resulted in significant reductions in dendritic length and complexity (Fig. 3B), as well as in spine density (Fig. 3C).

To substantiate these findings, we constructed adenoviral vectors to express either C3 along with enhanced green fluorescent protein (AdV-C3; eGFP-2A-C3 with CMV promoter) or eGFP alone as a control (Adv-GFP) (Fig. 3D). Upon transfection of Adv-C3 and Adv-GFP plasmids into cultured primary neurons, we observed a significant decrease in dendritic arborization length and complexity in the C3-overexpressing neurons (Fig. S3H). To corroborate these results in an *in vivo* setting, we performed stereotaxic injections of the prepared adenoviruses (Adv) and retro-RFP viruses into the bilateral hippocampal dentate gyrus of 8-week-old mice (Fig. 3E). Two weeks after injection, a subset of mice was euthanized to obtain unfixed hippocampal tissues. C3 overexpression was confirmed through immunoblotting of hippocampal lysates (Fig. 3F). Consistent with our previous findings, the dendritic length and complexity (Fig. 3G), as well as spine density (Fig. 3H) of RFP^+ newborn neurons in the C3-

overexpressing group were significantly reduced.

To assess the cognitive implications of C3 overexpression, we conducted behavioural assays 4-6 weeks post-Adv injection (Fig. 3E). During the open field test, mice overexpressing C3 covered significantly shorter total distances compared to controls (expressing eGFP alone), indicative of diminished locomotor activity. In C3-overexpressing mice, movement tracking revealed a strong preference for peripheral and corner locations, suggesting an increased level of low curiosity-like behaviour (Fig. 3I). In the novel object location (NOL) test, these mice showed less preference for object placement, suggesting an impaired spatial memory (Fig. S3I). Similar results were observed in the novel object recognition (NOR) test (Fig. S3J). Moreover, in the Morris water maze (MWM) (Fig. 3J) and reversal Morris water maze (RMWM) tasks (Fig. 3K), C3-overexpressing mice exhibited fewer platform crossovers, longer escape latencies (Fig. 3J and 3K) and less time in the target quadrant (Fig. S3K and 3L), compared to the control group. To be note, no obvious difference of the swimming ability was observed between the two groups (Fig. S3K and 3L). These behavioural changes induced by C3 overexpression were highly consistent with those observed in mice treated with hsAQP4-IgG.

Knockdown of C3 secreted by astrocytes improves adult hippocampal neuronal development and function in immune-mediated neuroinflammation.

To validate the critical role of C3 in the immune-mediated abnormal development of newborn neurons and cognitive impairments in vivo, we initially designed two shRNA sequences targeting C3. They were transfected into primary astrocytes using lentivirus (Lenti-shC3_1 and Lenti-shC3_2), along with a non-targeting control shRNA (shNC), respectively (Fig. S4A). Co-expression of EGFP was used to ensure efficient lentiviral transduction, achieving at least 95% efficiency. The effectiveness of C3 knockdown was confirmed by comparing the levels of C3 protein in primary astrocyte transduced by Lenti-shNC or Lenti-shRNA, with Lenti-shC3_2 being selected for subsequent experiments (Fig. S4A).

Primary astrocytes infected with either Lenti-shNC or Lenti-shC3_2 was treated with hsCtrl-IgG or hsAQP4-IgG, respectively, for an additional two days. The astrocyte-conditioned media (ACM) was then collected and assessed for its impact on primary neuronal dendritic development (Fig. S4B). In control groups, ACM from hsAQP4-IgG-treated astrocytes markedly reduced dendritic length and complexity (Fig. S4C). However, in the C3 knockdown groups, ACM from hsAQP4-IgG-treated astrocytes no longer inhibited neuronal dendritic arborization (Fig. S4C).

To verify the impact of C3 deficiency on the development of newborn neurons in adult mice, we utilized AAVs specifically targeting astrocytes. AAV2/5-GfaABC1D-EGFP (AAV-shNC) or AAV2/5-GfaABC1D-shRNA-EGFP (AAV-shRNA) was injected into the hippocampal dentate gyrus of 8-week-old mice (Fig. 4A). In these mice, shRNA was specifically expressed in astrocytes under the control of the GfaABC1D promoter, leading to C3 depletion in astrocytes of the hippocampal dentate gyrus (Fig. 4A). The effectiveness of C3 knockdown was confirmed through immunoblotting of hippocampal lysates, with a knockdown efficiency of over 90% (Fig. 4B). We co-injected AAV2/5-GfaABC1D-shRNA-EGFP and retrovirus along with hsAQP4-IgG into the dentate gyrus (DG) and mice were sacrificed four weeks after the injection. Adeno-associated virus co-expressing shRNA and GFP enabled C3 knockdown in astrocytes, while retroviruses expressing RFP allowed the labelling of newborn neurons (Fig. 4C). In each hippocampal section of 80 μm thickness, an average of 12

neuronal cells were labelled with retrovirus and expressed red fluorescent protein, indicating that they were newborn neurons (Figure 4D). Remarkably, C3 knockdown in astrocytes led to improvements in dendritic length and complexity (Fig. 4E), as well as in spine development (Fig. 4F).

Hippocampal-dependent learning and memory were subsequently assessed using OFT, NOL, NOR, MWM, and RMWM tests (Fig. 4C). C3 knockdown reversed low curiosity-like behavior in the OFT (Fig. 4G), enhanced preference for the novel object in the NOL and NOR tests (Fig. S4D and E), and led to significant decreases in escape latency and retention time, accompanied by an increased number of platform crossings and more exploration time in the target quadrant in both the MWM (Fig. 4H and Fig. S4F) and RMWM (Fig.4I and Fig. S4G) tasks, while the average swimming speed revealed no significant difference in the swimming ability among the groups (Fig. S4F and 4G). In summary, these studies provide convincing evidence for the inhibitory role of C3 secreted by immune-mediated activated astrocytes on hippocampal functions.

C3 cooperates with the C3aR receptor to inhibit adult hippocampal neuronal development by reducing β-catenin signalling.

To clarify the mechanism by which C3 signalling impairs hippocampal newborn neurons development in immune-mediated neuroinflammation, we attempted to identify the C3 receptor and downstream pathways in adult-born neurons. Previous studies have shown that upon the binding of C3 to its transmembrane receptor C3aR, several signalling cascades were activated (Figure 5A). To prove the expression of C3 receptors in adult-born hippocampal neurons, we used immunostaining to analyse the expression pattern of C3aR in the dentate gyrus of 8-week-old mice. Surprisingly, C3aR was abundantly expressed in DCX^+ immature neurons and mature granular cells (Fig. 5B). C3aR has also been confirmed to be highly expressed in cultured primary neurons (Fig 5C). After recognizing C3aR as a potential C3 receptor on primary neurons, we investigated the specific downstream pathways mediated by GSK3β and β-catenin (Fig. 5A). β-Catenin is a crucial transcription factor in the Wnt signalling pathway, regulating the development of neurons in the adult hippocampus. GSK3β, a serine/threonine protein kinase stimulated by C3aR activation, phosphorylates and targets β-catenin for proteasomal degradation. Notably, the kinase function of GSK3β can be inactivated by phosphorylation at Ser9. We detected the expression of GSK3β and β-catenin in primary mouse neurons treated with recombinant C3 protein (100 ng/mL). Remarkably, 2 hours of C3 protein treatment resulted in a rapid accumulation of active GSK3β, with a concomitant reduction in the inactivated form of GSK3β [p- GSK3β (Ser9)] (Fig. S5A). Besides, C3 treatment induced a sustained reduction in β-catenin protein levels lasting for over two hours (Fig. S5A), indicating destabilization and degradation of β-catenin triggered by increased GSK3β kinase activity, which can be recognized as the direct downstream pathway of C3-C3aR signaling.

To confirm the participation of C3aR as a receptor in the identified C3 signalling pathway, we designed three shRNAs targeting C3aR (shC3aR_1; shC3aR_2; shC3aR_3) and a scrambled non-targeting control shRNA (shNC). We then lentivirally transduced them individually into cultured mouse primary neurons, with co-expression of EGFP to ensure adequate transduction efficiency, >99%. The shRNAs designed all showed a satisfactory knockdown efficiency ranging from 75-90% (Fig. S5B). Furthermore, we also transfected primary hippocampal neurons with shNC or shC3aR and performed immunofluorescence staining to verify the knockdown effectiveness of C3aR in neurons (Fig S5C). After exposing primary

neurons to C3 for two hours, the expression of the inactivated form of GSK3β [p- GSK3β (Ser9)] in the shC3aR group was significantly elevated compared to the shNC group, thus preventing the degradation of β-catenin (Fig. 5D). Therefore, we came to the conclusion that C3aR depletion blocked the C3 effects on GSK3β activation and β-catenin inhibition. Besides, consistent with our in vitro results, we found a similar C3aR knockdown effect on GSK-3β/β-catenin pathway stimulated by C3 in vivo (Fig. S5D). Furthermore, we continued to explore whether C3aR-dependent signaling would be essential for inhibiting neuronal dendritic development induced by C3. In primary neuron cultures expressing control shRNA, C3 treatment reduced neuronal dendritic length and complexity. However, primary neurons deficient in C3aR due to shRNA displayed unchanged dendritic length and complexity (Fig. 5E). In summary, we proved that the binding of C3 to its receptor C3aR activates GSK-3β, which in turn destabilizes β-catenin and disrupts the transcriptional network related to neuronal development driven by β-catenin.

Subsequently, we evaluated whether C3 regulates neuronal development through its binding to C3aR *in vivo*. To interrupt the subsequent activation of signalling pathway induced by the bindng of C3 to C3aR, we injected retroviruses expressing control shRNA (shNC) or validated shRNA against C3aR into the hippocampal dentate gyrus of 8-week-old mice. These retroviruses have been shown to target neurons and reduce the expression of C3aR in neurons (Fig 5F). Two weeks after injection of retrovirus, we implanted a mini-pump for two weeks perfusion of PBS or C3 protein to evaluate neuronal dendritic and spine development (Fig. 5G). In the control group (shNC), C3 markedly reduced neuronal dendritic length and complexity (Fig. 5H), as well as spine density (Fig. 5I). By contrast, C3aR knockdown eliminated such repressive effects of C3, resulting in minimal or no observable impact on the development of neuronal dendrites and spines (Fig. 5H and I). Next, we investigated whether knockdown of C3aR could also prevent newborn neuronal dendritic development defects with hsAQP4-IgG treatment (Fig. S5E). As expected, knockdown of C3aR counteracted the inhibitory effect of dendritic arborization and spine development from hsAQP4-IgG (Fig. S5F and 5G). Altogether, our findings confirmed the damaging effect of C3-C3aR signalling on the newborn neuronal development in the dentate gyrus and suggested that inhibiting the C3-C3aR-GSK-3β/β-catenin pathway can be a potential therapeutic strategy to rescue impaired neuronal development in immune-mediated neuroinflammatory diseases.

Finally, we investigated the effect of the C3-C3aR signalling pathway on neuronal development by utilizing C3aR antagonists. Trifluoroacetate (SB290157, TFA) is the first reported C3aR antagonist that has been shown to inhibit Ca^{2+} mobilization induced by C3a binding to C3aR in mice (Ames *et al.*, 2001; Reid *et al.*, 2014). In addition, TFA is also a potent, selective, and non-competitive C3aR antagonist that has been widely used. We first stereotactically injected a mixture of hsAQP4-IgG and retroviruses expressing red fluorescent protein (RFP) to label newly generated neurons in the dentate gyrus of 8-week-old mice. After the injection, mice were intraperitoneally administered with TFA at a dosage of 1 mg/kg or vehicle as a negative control daily for a duration of four weeks (Fig. 5J). We found that TFA relieved the repression of neuronal dendritic arborization (Fig. 5K) and spine development (Fig. 5L) in the neuroinflammatory state triggered by hsAQP4-IgG. TFA treatment also reversed low curiosity-like behavior in the OFT (Fig. S5H) and increased preference for the novel object in the NOL (Fig. S5I) and NOR (Fig. S5J) tests. In addition, TFA treatment resulted in a significant decrease in escape latency, an increased number of platform crossings and more time spent in the target quadrant in the MWM (Fig. 5M and Fig. S5K) and RMWM (Fig. 5N and Fig. S5L) tasks. To be note, we noticed no difference in the

swimming ability among the groups (Fig. S5K and 5L).

Previous studies have shown that the C3-C3aR axis plays an important role in NMO through complex interactions among neurons, astrocytes, and microglia (Chen *et al.*, 2020; Wei *et al.*, 2021; Xu *et al.*, 2023). C3aR is also expressed in activated microglia (Davoust *et al.*, 1999; Wei *et al.*, 2021; Zhang *et al.*, 2014). To evaluate whether hsAQP4-IgG could mediate C3-dependent microglial immune responses and affect neuronal development, we sought to deplete microglia using PLX5622, an antagonist of colony-stimulating factor 1 receptor (CSF1R), which can kill microglia effectively. According to previous studies, PLX5622 treatment resulted in over 90% consumption of microglia within 7 days (Li *et al.*, 2023; Price *et al.*, 1987). In our study, mice received intraperitoneal injection of PLX5622 at a dosage of 50 mg/kg or vehicle daily and we observed a significant decrease in the number of IBA^+ microglial per DG in the PLX5622-treated group compared to the vehicle-treated group (Figure S6A), indicating a successful deletion of microglia. Despite the clearance of microglia, hsAQP4-IgG still reduced the neuronal dendritic length and complexity (Figure S6B), as well as the spine density of RFP^+ newborn neurons (Figure S6C). These findings indicated that microglia did not directly engage in the pernicious effect of hsAQP4-IgG-mediated neuroinflammation on neuronal development. Taken together, the results of genetic knockdown or pharmacological blockage of C3aR indicated that C3aR on neurons could be a potential target to interrupt the C3 signaling, which adversely affects hippocampal neuronal development after activation of astrocytes in immune-mediated neuroinflammation.

AAV2/9.CR2-Crry gene therapy ameliorates neuronal dendritic arborization developmental deficits and cognitive dysfunction in NMO mouse models.

Complement receptor 1-related gene/protein y (Crry) serves as an efficacious membrane-bound regulator of the complement C3 activation pathway, affecting both the classical and alternative routes (Atkinson *et al.*, 2005). Our prior investigations employing CR2-Crry demonstrated marked reductions in complement deposition and demyelination in various NMO models, including slice cultures and focal intracerebral injections. In systemic NMO mouse model, CR2-Crry treatment also reduced the production of pro-inflammatory cytokines and ameliorated motor dysfunction. Concurrently, utilizing serotype 2/9 adeno-associated virus (AAV2/9) to ensure stable expression of CR2-Crry ameliorated visual dysfunction by mitigating NMO-like lesions.

Prompted by these observations, we sought to examine whether AAV2/9-mediated delivery of CR2-Crry could rectify deficits in neuronal dendritic arborization and associated cognitive impairments. To this end, we performed stereotaxic injections of a mixture containing antibodies, retroviruses (retro-RFP), and AAV2/9.CR2-Crry into the dentate gyrus of 8-week-old mice (Fig. 6A). Remarkably, four weeks post-injection with hsAQP4-IgG treatment, we observed notable improvements in dendritic length and complexity (Fig. 6B), as well as in spine density (Fig. 6C) in retrovirus-labelled RFP^+ newborn neurons within the dentate gyrus of the AAV2/9.CR2-Crry-treated group.

Subsequently, we assessed hippocampal-dependent learning and memory using an array of behavioural assays: the open field test (OFT), novel object location (NOL), novel object recognition (NOR), Morris water maze (MWM), and reversal Morris water maze (RMWM) (Fig. 6A). Treatment withAAV2/9.CR2-Crry effectively reversed low curiosity-like behaviours observed in the OFT (Fig. S6D), enhanced preference for novel locations and objects in the NOL and NOR assays (Fig. S6E and 6F), and led to a significant reduction in escape latency

and retention time, accompanied by an increase in the number of platform crossings and more exploration time in the target quadrant both in the MWM (Fig. 6D and Fig. S6G) and RMWM (Fig. 6E and Fig. S6H) tasks. Notably, we noticed no difference in the swimming ability among the groups (Fig. S6G and Fig. S6H).

Regulation of GSK3-3β/β-catenin signalling pathway rescues newborn neuronal developmental deficits and cognitive dysfunction in NMOSD mouse models.

In an effort to corroborate the role of GSK3β and β-catenin in the C3 signalling cascade, we employed specific modulators of this pathway: the GSK3β inhibitor TWS119 and the β-catenin agonist BML-284. We examined their impact on hippocampal neuronal development and cognitive function in NMO mouse model of immune-mediated neuroinflammation.

Initially, we observed that treatment with either TWS119 (1 μM/mL) or BML-284 (1 μM/mL) effectively neutralized the C3-induced suppression on dendritic development in cultured primary hippocampal neurons (Fig. S7A). To extend these *in vitro* findings, we administered TWS119 (30 mg/kg) or BML-284 (4 mg/kg) via intraperitoneal injection in 8-week-old mice following stereotaxic administration of a mixture of hsAQP4-IgG and retro-RFP (Fig. 7A). Subsequently, RFP labelled neurons were employed to assess neuronal development. Remarkably, both TWS119 and BML-284 administration significantly elevated neuronal dendritic length and complexity (Fig. 7B), as well as spine density (Fig. 7C).

Further evaluation of hippocampal-dependent learning and memory was conducted using a battery of behavioural assays: the Open Field Test (OFT), Novel Object Location (NOL), Novel Object Recognition (NOR), Morris Water Maze (MWM), and Reversal Morris Water Maze (RMWM) (Fig. 7A). Both TWS119 and BML-284 treatments reversed low curiosity-like behaviour in the OFT (Fig. S7B), increased preference for novel objects and locations in the NOL and NOR tests (Fig. S7C and 7D), and significantly reduced escape latency and retention time, accompanied by an increase in platform crossings and more exploration time in the target quadrant in the MWM (Fig. 7D and Fig. S7E) and RMWM (Fig. 7E and Fig. S7F) tasks. Meanwhile, we observed no difference in the swimming ability among the groups (Fig. S7E and 7F).

Collectively, these findings provide compelling evidence that the C3-mediated signalling cascade cooperates with C3aR to inhibit adult hippocampal neuronal development through the GSK3β/β-catenin pathway in NMOSD mouse model (Fig. 7F).

Discussion

Neuromyelitis Optica Spectrum Disorders (NMOSD) is an autoimmune neuroinflammatory disorder characterized by immune-mediated demyelination and inflammation primarily targeting spinal cord, optic nerve and brain (Ma *et al.*, 2020). Such circumstances lead to severe neurological impairments including motor dysfunction, visual loss and cognitive decline, among others (Czarnecka *et al.*, 2020; Jiang *et al.*, 2023; Lopez-Soley *et al.*, 2022). Convincing evidence suggests the importance of innate immunity and neuroinflammation in NMO and relevant neuroimmune diseases. Our group have previously demonstrated that inhibition of astrocyte-secreted C3 signaling can ameliorate motor and visual dysfunction (Xu *et al.*, 2023). In this study, we found that the levels of C3a, a cleavage product of C3, significantly correlated with cognitive impairment in our patient cohort. Based on clinical, serological, and immunohistochemical research, we proposed that C3, a core component of the complement cascade, may influence dendritic and synaptic alterations in adult-born neurons within the dentate gyrus. These alterations contributed to the early-stage cognitive impairments observed in experimental NMO mouse models. We also found that dysregulation of astrocyte-newborn neuron interactions via the C3-C3aR-GSK3β/β-catenin pathway led to impaired dendritic development and hippocampal-dependent learning functions (Fig. 7F).

Previous studies have reported an increase in complement protein expression and activation of complement signalling in NMO patient autopsy tissue and hsAQP4-IgG passive transfer mouse models (Asavapanumas *et al.*, 2021; Carpanini *et al.*, 2019). Our RNA transcriptome analysis and immunostaining confirmed that C3 is mainly expressed in activated astrocytes, and its expression is further upregulated when hsAQP4-IgG is introduced, both in vitro and in vivo. This finding aligned with previous reports (Chen *et al.*, 2020). In the burgeoning field of complement therapeutics, various strategies targeting C3 activation have been proved to be effective and are currently being extended to human diseases, including those in clinical trials such as compstatin (López de Victoria *et al.*, 2011; Mastellos *et al.*, 2019). This cyclic peptide inhibits the binding of C3, thereby interfering with convertase formation and C3 cleavage (López de Victoria *et al.*, 2011). Complement receptor 2 (CR2)-Crry is a fusion protein targeting sites of complement activation, which blocks all pathways of C3 activation step (Atkinson *et al.*, 2005). The mouse complement-inhibitory protein Crry, is directed through its CR2 fusion partner, which binds to C3d, a cell-bound complement activation product deposited at the sites of complement activation(Atkinson *et al.*, 2005; Xu *et al.*, 2023). CR2-Crry has shown neuroprotective effects in ischemic brain models (Alawieh *et al.*, 2015) and in the experimental autoimmune encephalopathy model of multiple sclerosis (Hu *et al.*, 2012). Traumatic brain injury mouse models treated with continuous CR2-Crry exhibited improved spatial learning and memory performance (Alawieh *et al.*, 2018). Our previous research has demonstrated that CR2-Crry has the ability to prevent the motor and visual deficits observed in NMO models (Xu *et al.*, 2023). Our current study also demonstrated that using AAV2/9 to deliver CR2-Crry effectively improved hippocampal neuronal arborization and cognitive function in NMO mouse models.

The activation of C3 is the common pathway for all three pathways of complement activation, resulting in the cleavage of C3 into fragments like C3a and C3b by C3 convertase. C3a acts as an anaphylatoxin and binds to its receptor C3aR to trigger downstream biological effects (Minton, 2014). Notably, prior research has implicated complement alternative pathway-activated C3-C3aR signalling in demyelination and neurodegeneration. Microglia

and astrocytes are recognized as the primary producers of complement C3 secretion, with neurons, endothelial cells, and oligodendrocytes serving as additional contributors. Under physiological conditions, neuronal and synaptic function can also be mediated by astroglia C3-neuron-glia interactions (Lian *et al.*, 2016). During the early stages of postnatal development, the brain exhibits notable expression of C3 and C1q complement proteins, with C3aR playing a role in controlling migration and differentiation of neural progenitor cells (Pozo-Rodrigálvarez *et al.*, 2021). Previous research has shown that TNF-α boosts C3 mRNA levels and that augmented astroglial NFκB/C3/C3aR signalling facilitates AMPAR membrane localization, thereby increasing synaptic strength (Stellwagen and Malenka, 2006). Aβ triggers NFκB activation in astrocytes and the secretion of C3, which then enhances synaptic excitation and disrupts dendritic development via neuronal C3aR and intracellular calcium, causing network dysfunction (Lian *et al.*, 2015b). This model connects Aβ to synaptic impairments and increased neuronal excitability via a new neuron-glia signaling pathway, highlighting the astroglial IκBα/NFκB regulatory loop and complement activation as key components in the development of AD (Lian *et al.*, 2015b). Our results validated that astroglial levels of complement C3 were increased by stimulation of hsAQP4-IgG. While this pathway is elevated in NMO mouse models and patient brain samples, we demonstrated that blocking C3aR ameliorated behavioural impairments in NMO mouse models. These results are consistent with previous studies reporting a general neuroprotective effect through the inhibition of complement activation. C3aR, a G protein-coupled receptor, seems to be a potential target for pharmaceutical intervention, particularly since mice with complete C3aR deficiency exhibit normal behaviors (Humbles *et al.*, 2000). Using trifluoacetate (TFA) to block C3aR mitigated anxiety and learning deficits in NMO mouse models. Blocking C3aR also reversed the decrease in dendritic length and complexity, as well as the loss of dendritic spines in mice with NMO. These findings reflected the integrated molecular mechanism whereby abnormally high levels of C3 act on C3aR to induce synaptic injury. However, obtaining human hippocampal samples has proved to be challenging, prompting us to rely solely on mouse hippocampal samples to investigate the molecular pathways underlying NMO cognitive impairments. Therefore, C3aR remains an attractive target for intervention in NMO.

Mechanistically, we identified GSK3β/β-catenin as a downstream effector of C3aR. The GSK3β/β-catenin pathway has been extensively studied in the context of neural development regulation. Emerging evidence suggests that GSK-3β, an essential kinase for cellular communication and a negative regulator of the canonical Wnt signalling pathway, is crucial in regulating various neurodevelopmental processes, such as neurogenesis, neuronal polarization, axonal growth and guidance, and neuronal migration (Chenn and Walsh, 2002; Herrera *et al.*, 2023; Hirabayashi *et al.*, 2004; Lie *et al.*, 2005; Murase *et al.*, 2002).

This study indicated that C3 overexpression had a negative impact on spatial cognitive ability in mice and reduced the phosphorylation of Ser9 of GSK-3β and β-catenin levels in the hippocampus. However, blocking GSK-3β significantly ameliorated the cognitive impairments caused by hsAQP4-IgG, highlighting the importance of GSK-3β/β-catenin pathway in cognitive impairments related to NMO. In summary, our research demonstrated the importance of C3/C3aR-GSK3β/β-catenin in regulating immune homeostasis in the central nervous system and adult-born hippocampal neuronal development through targeting the GSK3β/β-catenin signalling network. We proved a connection between the C3-C3aR pathway and GSK3β signalling, providing novel insights into targeting this pathway for potential therapeutic strategies in NMO.

MATERIALS AND METHODS

Animals

Each experiment utilized adult C57BL/6 mice aged 8-12 weeks, obtained from Vital River for each specific trial. The analysis of mouse behaviour took place at the Guangdong Institute for Monitoring Laboratory Animals. The mice were kept in an environment that was free of specific pathogens, maintained at a consistent temperature, and subjected to a 12-hour cycle of light and darkness. Every mouse in the cage had unrestricted access to food and water. The animals were randomly assigned to experimental groups. Before the completion of the experiment, the experimenter was blinded to the animal assignments. Procedures and feeding followed approved protocols from the Laboratory Animals Monitoring Institute and the animal experiment ethics committee of the Third Affiliated Hospital of Sun Yat-Sen University.

Primary astrocyte culturing and treatments for the collection of ACM

Primary astrocyte culture from mice was conducted following the methods outlined in the publications by Huang et al. in 2017(Huang *et al.*, 2017) and 2019(Huang *et al.*, 2019). Mouse pup brains aged P0-P1 were harvested briefly. Following the removal of the meninges, the brain underwent three washes in cold DMEM-F12 (C11330500BT, GIBCO) supplemented with 10% FBS (ST30-3302, PANTM SERATECH) and 1% penicillin streptomycin (15140-122, GIBCO). The tissue was moved to a solution of 0.25% trypsin EDTA (25200072, GIBCO) and left to incubate at 37°C for 20 minutes, with periodic gentle shaking every 5 minutes. The trypsinization process was stopped by mixing in an equivalent amount of DMEM-F12 full medium. To obtain a single-cell suspension, the sample was filtered through a 40 μm nylon mesh to eliminate cell debris and clumps, then centrifuged at 1000g for 5 minutes. The last suspension of individual cells was mixed again in DMEM-F12 (C11330500BT, GIBCO) with 10% FBS (ST30-3302, PANTM SERATECH), 1% NEAA (M7145, MACKLIN), 1 mM sodium pyruvate (S8636, Sigma), 1% glutamine (25030-081, GIBCO), and 1% penicillin streptomycin (15140-122, GIBCO) before being placed in T75 flasks (one mouse brain per T-75 flask, each with a total volume of 10 mL) for a period of 10 days. Incubation of the cells at 37°C with 5% CO2 allowed for adhesion to occur. The medium was changed every 3 days, allowing the mixed glial cells to reach full coverage. On the 10th day, gently wash the mixed glial cells in the T75 flask with PBS to remove floating cells. Then attach the T75 flask to a thermostatic shaker and shake for 16 hours (37°C, 250 rpm). Afterward, discard the medium containing suspended cells. Currently, at the bottom of the culture flask, there is a layer of intact astrocytes with some oligodendrocytes scattered on the surface. Astrocytes have a purity of 95%, determined by analysing the expression of GFAP (1:1000, CST, 12389S) as a biomarker.

To collect ACM, primary mouse astrocyte culture was treated with either hsCtrl-IgG or hsAQP4-IgG at 100 ng/mL for 24 hours. Then replace with complete astrocyte culture medium and continue to culture for 24 hours, collecting astrocyte condition medium (ACM). Cell fragments in the ACM were filtered out using a 0.22 μm nylon grid (BS-QT-037, Biosharp). Add 100 ng/mL of anti-C3 monoclonal antibody (V3S-0522-YC3020, Creative Biolabs) to the filtered ACM to remove C3 secreted by astrocytes, and then use the cleared ACM to culture primary neurons for 3 days. After 3 days, the cells were fixed and immunofluorescence staining was conducted to evaluate neuronal development.

Isolation and transfection of primary neurons in mice

Hippocampal neurons from mice were separated and transfected according to the method described in reference (Tang and Guo, 2021). Primary hippocampal neurons were obtained from mouse pups on postnatal days 0 to 1 (P0-P1). P0 mice were decapitated, their hippocampal tissue extracted, and then placed in DMEM medium with 3% penicillin streptomycin. After centrifuging the tissue at 1000 revolutions per minute at room temperature for 2 minutes, the liquid above was removed, and 2 millilitres of 0.125% trypsin (25200-056, GIBCO) chilled on ice was poured onto the tissue block for digestion in a 37°C warmer for 15 minutes. The digestion process was stopped using N2A solution, which consisted of DMEM-F12 with 10% FBS and 1% penicillin streptomycin. The tissue block was drawn into a new 1 mL N2A medium and pipetted approximately 15 times. The suspension was allowed to settle for 1-2 minutes, and the sediment was transferred into another tube containing 1 mL of N2A medium and pipetted approximately 15 times. Combining the suspensions allows for the seeding of hippocampal neurons into 4-6 wells of a 24-well plate, each receiving an extra 500 µL of N2A culture medium. After 4 hours, the culture medium was changed to a specialized medium for neurons, which included 2% B-27 supplement (17504-044, GIBCO), 1% penicillin streptomycin, 1% glutamine, and Neurobasal (21103049, GIBCO). The neuron culture medium was replaced every other day.

One hour before transfection, the original culture medium was discarded, and each well received 300 µL of neuron culture medium without penicillin streptomycin. In two tubes, 1 microgram of plasmids and 1 µL of Lipofectamine 2000 (2477064, Invitrogen) were combined with 50 µL of Opti-MEM medium, then left at room temperature for 5 minutes. The two options were merged, thoroughly blended, and left to sit at room temperature for 20 minutes. Each well received 100 microliters of the mixture and was then gently agitated. For the statistical analysis of dendritic morphology, transfections were carried out on the second day in vitro. Four hours post-transfection, the entire culture medium was replaced, and cells were fixed after 7 days.

Obtaining IgG from humans and mice

Autoantibodies targeting AQP4 (hsAQP4-IgG) were isolated from combined plasma samples of NMO patients positive for anti-AQP4 antibodies (hsAQP4-IgG) or from healthy individuals (hsCtrl-IgG) using protein A beads (71149800, GE Healthcare). After washing the beads with 100 mM glycine HCl (pH 2.5), the elution was concentrated with an Amicon Ultra 15 centrifugal filtration unit (100k, Millipore). Concentrated antibodies were assessed for purity through SDS-PAGE analysis and their concentration was determined with a Pierce BCA protein assay kit (23225, Thermo Fisher).

ELISA analysis of C3, C3a, C3b levels

Purified astrocytes were exposed to hsCtrl-IgG and hsAQP4-IgG at a concentration of 100 ng/mL for 24 hours to induce secretion of C3 protein into the astrocyte-conditioned medium, followed by collection of the supernatant. C3 (Jiangsu Meimian Industrial Co., Ltd, MM-44699M1), C3a (Jiangsu Meimian Industrial Co., Ltd, MM-0906H1) and C3b (Jiangsu Meimian Industrial Co., Ltd, MM-45658M2) levels were measured using a commercial ELISA kit.

Western Blot

For Western blot analysis, the cell sample was thoroughly mixed with cell lysis buffer (P0013, Beyotime) and simultaneously supplemented with 1% protease inhibitor (P1006, Beyotime) and phosphatase inhibitor (P1045, Beyotime). BCA Protein Assay Kit (P0012S, Beyotime) was

then used to determine the sample concentration, and samples were mixed with 5 X SDS-PAGE sample loading buffers (P0015, Beyotime). The specimens were placed on 10% SDS-PAGE gels and then moved to polyvinylidene fluoride (PVDF) membranes. Protein bands were visualized using a Tanon 5500 system. Band intensity was quantitatively evaluated using ImageJ software. Blots were obstructed with 5% milk in Tris-buffered saline with Tween-20 and then exposed to rabbit anti-C3 (1:500, Thermo Fisher Scientific), mouse anti-C3aR (1:500, Santa Cruz Biotechnology), rabbit anti–GSK-3β (1:1000, Bioss), rabbit anti–p-GSK-3β (1:1000, CST), rabbit anti–β-catenin (1:1000, CST), and mouse anti–β-actin (1:1000, Huabio).

Production of lentivirus and retroviruses

The production of lentivirus and retrovirus was carried out according to the method described in a previous study(Tang and Guo, 2021). Cultured HEK293T cells in DMEM with 10% FBS and 1% penicillin-streptomycin until they reached 70% confluence. Vectors for packaging and Opti-MEM reduced serum medium (2276989, Gibco) were mixed together in a 5 mL total volume and left at room temperature for 5 minutes. Simultaneously, polyethyleneimine (PEI, PR40001, Proteintech Group) was mixed with Opti-MEM in a total volume of 5 mL and incubated for 5 minutes. After combining these solutions, they were incubated at 37°C for 20 minutes before being co-transfected into HEK293T cells. For retrovirus production, packaging plasmids were replaced with CMV-GP and VSVG. Medium was changed 4–6 hours after either lentivirus or retrovirus infection. At 48, 72, and 96 hours after transfection, medium containing the virus was gathered, passed through a filter (BS-250-XT, Biosharp), and then concentrated using ultracentrifugation (Beckman SW32 Ti) to reach concentrations ranging from 10^8 to 10^9. The virus was resuspended in 100 µL DPBS and stored at -80°C.

BML284, TWS119 trifluoroacetate (SB290157, TFA) and PLX5622 administration

BML-284 (HY-19987, MedChem Express, 4 mg/kg) is a potent, cell-permeable Wnt signalling activator that significantly induces the expression of β-catenin with an EC50 of 700 nM. The compound TWS119 (HY-10590, MedChem Express, 1 mg/kg) acts as a specific inhibitor of GSK-3β and has an effect on the WNT/β-Catenin signalling pathway as well. SB290157 trifluoroacetate (HY-101502A, MedChem Express, 1 mg/kg) is a potent, selective C3a receptor antagonist with an IC50 of 200 nM. These compounds were administered via intraperitoneal injection (i.p.) every other day for 4 weeks. PLX5622 (1303420-67-8, KKL, 50 mg/kg) is a highly selective brain penetrant and orally active CSF1R inhibitor (IC50=0.016 µM; Ki=5.9 nM). PLX5622 allows for extended and specific microglial elimination, preceding and during pathology development. PLX5622 demonstrates desirable PK properties in varies animals.

Establishing NMOSD systemic mouse models

Mice received subcutaneous injections of complete Freund's adjuvant (CFA) (Sigma-Aldrich) containing heat-killed H37Ra Mycobacterium tuberculosis (BD-DIFCO) (50 µg in 50 µL of CFA) seven days before retroviral and hsAQP4-IgG injection. The animals received i.p. injections (PTX, 200 ng in 0.2 mL of PBS, Enzo Life Science) 7 and 4 days prior to the hsAQP4-IgG transfer to disrupt the BBB, and systemic transfer of hsAQP4-IgG.

Stereotactic injection of mouse hippocampus

Stereotactic injection was carried out as described(Jiang *et al.*, 2023). Inhalation anaesthesia

was used to anesthetize mice between 8 and 12 weeks old, which were then secured on a stereotactic frame (RWD Life Science, Shenzhen, China). An injection of 1 µL, containing either virus or IgG, was administered into the dentate gyrus of the hippocampus over a period of 2 minutes per 1 µL. Subsequent tests were performed, and brain samples were collected for immunofluorescent staining. The needle for infusion was accurately placed in the DG with the specified coordinates from Bregma: -2.0 mm anteroposterior; ± 1.7 mm lateral; -1.9 mm ventral.

Adenovirus Gene and Adeno-associated virus transfer

Adenoviral vector encoding the mouse C3 gene (Adv-C3) and negative control (Adv-GFP) was constructed, packaged, purified, and titrated at Genechem Co. Ltd. For adenovirus-mediated gene transfer, the overexpression efficiency of Adv-C3 was evaluated by Western-blot. To evaluate the effect of C3 on neuronal development, AAV-shC3 or AAV-shGFP was injected for behavioral testing, and the knockdown efficiency of AAV-shC3 was assessed using Western blotting. Adeno-associated virus purchased from Shandong Weizhen Biotechnology Co., Ltd, selection pAV-GfaABC1D-P2A-GFP astrocyte specific promoter GfaABC1D initiates target gene expression, target gene ATG is preceded by kozak sequence GCCAAC, target gene and GFP are expressed non fused through P2A. AAV2/9-CMV-EGFP and AAV2/9-CMV-CR2-Crry-P2A-EGFP viruses were composed and purchased from Obio Technology (Shanghai, China).

Mini-osmotic pump grafting

A detailed procedure for hippocampal infusion via mini-osmotic pump was described in previously published methods (Jiang et al., 2023). Alzet mini-osmotic pumps of model 1002 were put together following the guidelines provided by the manufacturer, with a flow rate of 0.25 µL per hour for a duration of 14 days. Pumps containing either recombinant protein C3 or hsAQP4-IgG were immersed in 0.9% normal saline and left to incubate at 37°C for 12-16 hours. Next, they were placed at Bregma-relative coordinates of -2.0 mm anteroposterior; ± 1.7 mm lateral; -1.9 mm ventral.

Behaviour test

Open Field Test (OFT)

The mice were evaluated for their general movement and levels of anxiety using the open field test, following the method previously described (Wang and Cui et al., 2019). Mice from different experimental groups from the same position were placed in a square chamber (50×50×50 cm) for 10 minutes. The XinRuan software (XinRuan Information Technology Co., Shanghai, China) categorizes the mouse movement area into 9 sections, encompassing both central and outer areas. Record the average total travel distance and the average number of trips through the central area as indicators for evaluating mouse motor ability and anxiety behaviour.

Morris Water Maze (MWM) Test

The Morris Water Maze task was executed in accordance with the previously provided instructions(Vorhees and Williams, 2006). Briefly, the water maze is divided into four quadrants. Position a round platform measuring 10-12 cm in diameter approximately 1-2 cm beneath the surface of the water in the third section while keeping the water temperature at 22℃. Throughout the training period, mice were placed randomly in the water maze starting from four different positions (NE, NW, SE, and SW); all mice in the experiment were trained

four times daily for five consecutive days to locate the concealed platform in the third quadrant. During the last assessment, eliminate the platform and record the time it takes to escape in order to determine the number of times the platform is found and the number of times the platform quadrant is crossed in training sessions to assess short-term spatial memory. Each test was conducted daily at the same time.

Reverse Morris Water Maze (RMWM) Test

After the MWM test, the mice should rest for at least 48 hours according to the described protocol(Chen *et al.*, 2021). Move the platform to the opposite quadrant in the Morris Water Maze and train all mice four times a day for 3 days prior to the final assessment.

Novel Object Location (NOL) Test

The NOL test was performed as follows(Barker and Warburton, 2011). Every mouse had the opportunity to roam freely for a duration of 10 minutes on the initial day. The next day, each mouse was relocated to the arena for 10 minutes; two identical objects A were placed diagonally. Two identical objects B replaced objects A on the third day for a 10-minute training session. Objects B were arranged in parallel and observed for 10 minutes on the fourth day. The updated position preference was indicated by the proportion of time dedicated to exploring the new site compared to the overall duration. The researchers conducting the study were unaware of the genetic makeup of the mice.

Novel Object Recognition (NOR) Test

The examination was carried out as previously described(Matsumoto *et al.*, 2014). During the orientation session on the initial day, every mouse had the opportunity to investigate a pair of matching items for a duration of 10 minutes. The next day, each mouse was relocated to the enclosure for 1 minute and then placed back into the cage. At the same time, two identical items were positioned side by side in the area for a duration of 10 minutes (1 mouse per item). On the third day, place two identical objects C into the space in parallel for 10 minutes (1 mouse/time). On the fourth day, replace one object C with object D and record for 10 minutes. By utilizing two stopwatches to measure the time dedicated to investigating object C and object D, the updated position preference was determined by dividing the time spent exploring the unfamiliar object by the overall time. The researchers conducting the study were unaware of the genetic makeup of the mice. The object recognition index = Tnew/(Tfamiliar+Tnew), where Tfamiliar and Tnew represent the time spent with the familiar and new objects, respectively.

Immunohistochemistry for confocal imaging of mouse hippocampal slices

Immunofluorescence was conducted based on previously published protocols with certain modifications(Jiang *et al.*, 2023). Animals were anesthetized by intraperitoneal injection of 2% pentobarbital sodium. Gently open the mouse's chest cavity to reveal the heart, perfused with 30 mL ice-cold PBS, and then continue perfusion with 30 mL ice-cold 4% paraformaldehyde. After being immersed in 4% paraformaldehyde at 4℃ overnight, the brain was then placed in 30% sucrose for a minimum of 48 hours before being sliced into 40 or 80 μm sections using a freezing microtome. After being incubated overnight at 4℃ with specific primary antibodies diluted in PBS with 2% BSA, the slices were then incubated again overnight at 4℃ with primary antibodies. After being washed four times in PBS, the slices were incubated with secondary antibodies at room temperature for 1-2 hours. Subsequently,

their cell nuclei were stained with DAPI (2261b, Sigma Aldrich). We utilized the following antibodies: chicken anti-MAP2 (1:1000, Abcam), rabbit anti-NeuN (1:500, Abcam), rat anti-BrdU (1:1000, Abcam), rabbit anti-c-Fos (1:1000, CST), chicken anti-GFP (1:1000, Abcam), rabbit anti-RFP (1:500, MBL), mouse anti-DCX (1:200, Santa Cruz Biotechnology), and mouse anti-C3aR (1:200, Santa Cruz Biotechnology). Goat anti-chicken 488, goat anti-rabbit 488, goat anti-mouse 488, goat anti-rat 568, goat anti-rabbit 568, goat anti-mouse 568, and goat anti-rabbit 647 were the secondary antibodies employed in the study. All secondary antibodies were purchased from Invitrogen with a dilution ratio of 1:1000. The samples were observed and recorded with a Leica TCS SP8 laser confocal microscope that had four laser lines (405, 488, 568, and 647 nm) and objective lenses of 10×, 20×, 40×, and 63×.

Clinical data collection

We screened 90 patients with NMOSD participating in this retrospective study. Samples of serum and cerebrospinal fluid from individuals with NMOSD and from healthy participants were collected from two hospitals: The Third Affiliated Hospital of Sun Yat-sen University and The Second Affiliated Hospital of Guangzhou Medical University, with approval from all participants. Patients with NMOSD were identified based on the diagnostic criteria outlined in the 2015 International Panel for NMO Diagnosis (IPND). Neuropsychological evaluations and MRI images were obtained while the patients were in a stable clinical state, either recovering from an episode or free from relapse for a minimum of 3 months without any signs of symptomatic deterioration. The research was given the green light by the Ethics Committee at the Third Affiliated Hospital of Sun Yat-sen University, following the guidelines set forth in the Declaration of Helsinki.

MRI acquisition and hippocampal subfield volume analysis

A 3D fast spoiled gradient-echo sequence was used to scan all MRI data of the entire brain with a 3.0-T magnetic resonance system from Philips Medical System Ingenia scanner. The MRI data was obtained with a repetition interval of 7000 milliseconds, a flip angle of 90 degrees, an echo delay of 125 milliseconds, an acquisition matrix size of 272×176, and a slice depth of 6 millimetres. Automated segmentation and measurement of hippocampal subfields were performed with FreeSurfer 7.1.1 software, accurately identifying subfields including parasubiculum, presubiculum, subiculum, CA1, CA2/3, CA4, granular cell layer of DG, hippocampus-amygdala transition area, fimbria, molecular layer, fissure, and hippocampal tail.

Clinical screening

Demographic and clinical data, such as age, gender, education, and disease duration, were documented for both NMOSD patients and healthy controls. The Hamilton Depression Rating Scale (HDRS) and Hamilton Anxiety Rating Scale (HARS) were utilized to evaluate levels of depression and anxiety. Scores above 8 on the HDRS suggested potential depression, while scores above 20 indicated depression. HARS scores above 7 suggested potential anxiety, while scores above 14 indicated the presence of anxiety. The Mini-Mental State Examination (MMSE) is commonly utilized for evaluating the cognitive status of individuals and detecting conditions like dementia. In addition to the SDMT, the BVMT-R is another test that is utilized for identifying cognitive deficits. The tests have proven to be very responsive, simple to administer, and rapidly indicate the mental condition and level of cognitive decline in the subjects.

Statistical analysis

Prism 9.0 (GraphPad Software) was utilized to analyses the data. Values are presented as average ± SEM and statistical significance was defined as $p < 0.05$ (See each figure for details). The sample size was not pre-determined using statistical methods due to the unavailability of effect sizes prior to the experiments. Sample sizes can be found within figure legends. Pairwise comparisons were conducted using Student's t-test, while one-way or two-way analysis of variance (ANOVA) was followed by Tukey's post hoc test for sholl analysis or animal behavioural assays. Descriptive statistics were utilized to display demographic traits, while the correlation between neuropsychological assessments and C3 levels was analysed with the Pearson correlation coefficient. The importance was indicated by $*p < 0.05$, $**p < 0.01$, $***p < 0.001$, $****p < 0.0001$.

Figure legends

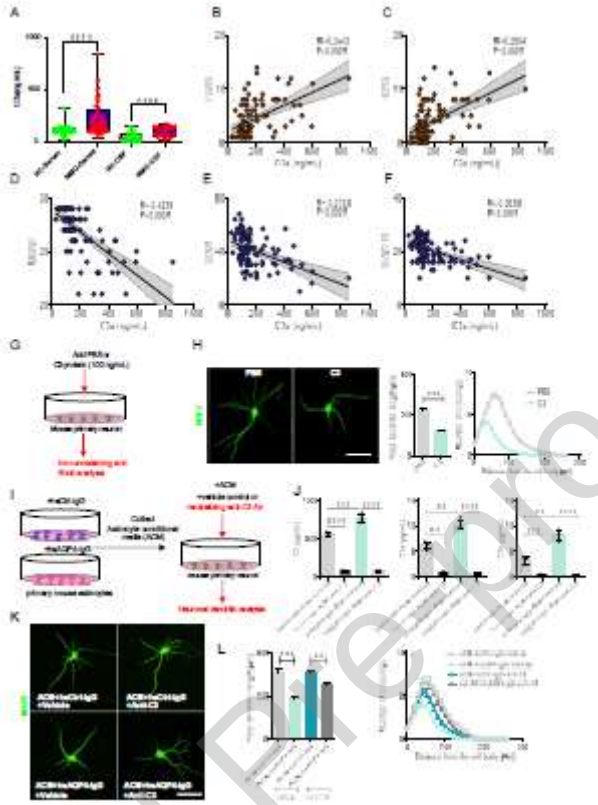

Fig.1 The effects of astrocyte-secreted C3 on hippocampal function and neuronal development

(A) Quantification of serum and CSF C3a levels in healthy controls (HCs) and NMO patients. HC-serum, n=50; NMO-serum, n=60; HC-CSF and NMO-CSF, n=30.

(B-F) The correlation between C3a serum levels and neuropsychological assessments in NMO patients. C3a levels positively correlated with increased anxiety and depression-like symptoms assayed by HARS (B) and HDRS (C) tests, and negatively correlated with cognitive performance in learning and memory functions assayed by tests of MMSE (D), SDMT (E), and BVMT-R (F).

(G) Schematic diagram for experiments to demonstrate the effect of C3 on primary neuronal development in vitro. The primary neurons were stimulated with recombinant C3 protein (100 ng/mL) or vehicle control of PBS for 3 days in the media and were then fixed and subjected to confocal analyses for neuronal development.

(H) Representative images of cultured primary hippocampal neurons with or without C3 treatment. MAP2 (green) marks the primary hippocampal neurons. Quantification of dendritic length (left bar graphs) and dendritic complexity (right broken-line graphs) of primary hippocampal neurons stimulated with PBS or C3 by Sholl analysis. n=30 neurons from 3 independent experiments. Scale bars, 50 μm.

(I) Schematic diagram for experiments to test the effect of astrocyte-secreted C3 on primary

hippocampal neuronal development. The primary cultures of mouse astrocytes were first treated with hsCtrl-IgG or hsAQP4-IgG at 100 ng/mL for 24 hours. The astrocyte-conditioned media (ACM) were harvested and treated with vehicle control or neutralizing anti-C3 antibodies (100 ng/mL) to eliminate the secreted C3 after removal of IgG contents. The cleared ACM were then supplemented with factors to constitute the growth media for primary hippocampal neurons. The mouse primary hippocampal neurons were cultured in ACM-based proliferation media for 3 days and, 3 days later, were fixed and immunostained for Sholl analyses of neuronal development.

(J) ELISA measurements of the secreted C3, C3a and C3b levels in ACM harvested from primary cultures of mouse astrocytes treated with hsCtrl-IgG or hsAQP4-IgG. n=3 experiments per group.

(K) Representative images of primary hippocampal neurons in 4 conditions—grown in hsCtrl-IgG-ACM or hsAQP4-IgG-ACM, Without (vehicle) or with C3 clearance (anti-C3)—immunostained with neural markers of MAP2 (green). Scale bars, 50 μm.

(L) Quantification of dendritic length (left bar graphs) and dendritic complexity (right broken-line graphs) of primary hippocampal neurons in the indicated 4 groups by Sholl analysis. n=30 neurons from 3 independent experiments.

Data in (A), (H), (J), and (L) were presented as the mean ± SEM; in (A), (H), and (J) statistical significance was evaluated with Student's t-test for two-group comparisons; statistical analyses of results in (L) were computed with one-way ANOVA and Tukey's post hoc multiple comparisons. For (H), dendritic complexity was evaluated with two-way ANOVA test; $p< 0.0001$. For (L), dendritic complexity was evaluated with two-way ANOVA test; hsCtrl-IgG-ACM+Vehicle vs. hsAQP4-IgG-ACM+Vehicle,$p<0.0001$; hsAQP4-IgG-ACM+Vehicle vs. hsAQP4-IgG-ACM+Anti-C3, $p < 0.001$. For (B-F), by Pearson correlation coefficient. Nonsignificant comparisons were not identified. *$p < 0.05$; **$p < 0.01$; ***$p < 0.001$; ****$p < 0.0001$.

Abbreviations: HC, healthy control; NMO, neuromyelitis optica; MMSE, Mini-Mental State Examination; SDMT, Symbol Digit Modalities Test; BVMT-R, Brief Visuospatial Memory Test Revised; HARS, Hamilton Anxiety Rating Scale; HDRS, Hamilton Depression Rating Scale.

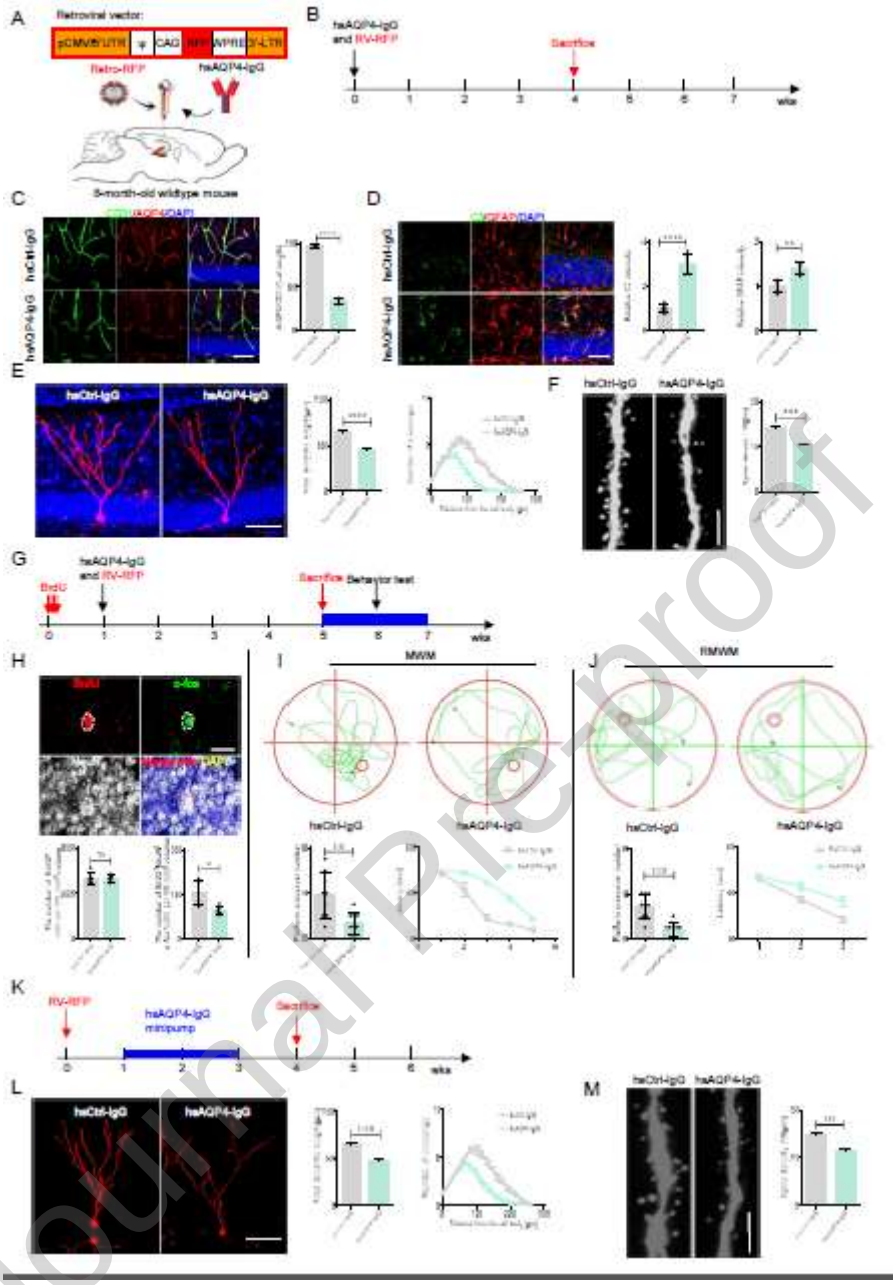

Fig. 2 The effects of immune-mediated astroglia activation on hippocampal neuronal development and cognitive performance

(A and B) Schematic diagram (A) and timeline (B) of the stereotaxic injection of retroviruses expressing RFP and hsCtrl-IgG or hsAQP4-IgG mixture.

(C) Representative confocal imagesalysis of AQP4 expression enriched within the astrocytic end-feet along the micro vessels in the hippocampal regions from mouse brains injected with hsCtrl-IgG or hsAQP4-IgG. The quantification was performed by calculating percentage of AQP4 coverage (green) along the length of micro vessels labelled by the endothelial marker CD31 (red). n=3 animals per group. Scale bar, 100 μm.

(D) Assessment of C3 expression in astrocytes induced by hsAQP4-IgG, quantified by the intensity of C3 fluorescence (green) that was colocalized with GFAP signals (red) and presented as the relative levels after setting the value of hsCtrl-IgG as 1.0. n=3 animals per

group. Scale bar, 50 μm.

(E) Representative confocal images and quantification of the dendritic length and dendritic complexity of RFP^+ newborn neurons in hsCtrl-IgG or hsAQP4-IgG treated adult mice 4 weeks after retrovirus injection. n=30 neurons per group from 6 mice. Scale bars, 50 μm.

(F) Representative confocal images (left) and quantification of dendritic spine density (right) of retrovirally infected newborn neurons in mice injected with hsCtrl-IgG or hsAQP4-IgG. n=30 neurons per group from 6 mice. Scale bars, 50 μm.

(G) Schematic diagram of assays for hippocampal newborn neurons (BrdU labeling) and cognitive performance with stereotactic injection of control (hsCtrl-IgG) or human anti-AQP4 antibody (hsAQP4-IgG). The IgG-injected mice were given 5-bromo-2'-deoxyuridine (BrdU) i.p. at 50 mg/kg for 4 consecutive days starting from one week before stereotactic injections.

(H) Representative confocal images (upper panel) of $BrdU^+NeuN^+c\text{-}Fos^+$ cells in the DG of mice, and quantification (lower panel) of the number of $BrdU^+$ cells, $BrdU^+NeuN^+c\text{-}Fos^+$ cells in the DG of mice injected with hsCtrl-IgG or hsAQP4-IgG. n=5 mice per group. Scale bars, 20 μm.

(I) Representative movement paths of the mice receiving hsCtrl-IgG or hsAQP4-IgG stereotactic injections in the standard MWM task. Quantification of the escape latencies to find the platform and the platform quadrant crossing numbers during the training sessions in the MWM task for both tested groups. n=9 animals per group.

(J) Representative reverse RMWM movement paths of the indicated groups. Quantification of RMWM escape latencies to find the platform and platform crossing numbers. n=9 animals per group.

(K) Timeline of the experiments for mini-pump infusion of hsCtrl-IgG or hsAQP4- IgG and analyses of RFP^+ newborn neurons.

(L) Representative images of RFP^+ newborn neurons in hsCtrl-IgG mini-pump or hsAQP4-IgG mini-pump treated mice 1 week after retrovirus injection. Quantification of the dendritic length and dendritic complexity of the indicated groups by Sholl analysis. Scale bars, 50 μm. n=30 neurons from 6 mice.

(M) Representative confocal images (left) and quantification (right) of dendritic spine density of retrovirally infected newborn neurons in mice with mini-pump infusion of hsCtrl-IgG or hsAQP4-IgG. Scale bar, 50 μm. n=30 neurons from 6 mice.

All the bar graphs were presented as the mean ± SEM. For data in (C-F), (H-J), (L) and (M) the statistical significance was evaluated with Student's t-test for two-group comparisons. For (E) and (L), dendritic complexity was evaluated with two-way ANOVA test. For (E), $p < 0.0001$. For (L), $p < 0.0001$. For (I) and (J), significance was evaluated with two-way ANOVA and Tukey ’s multiple-comparisons test. For (I), $p < 0.001$. For (J), $p < 0.01$. Nonsignificant comparisons were not identified. *$p < 0.05$; **$p < 0.01$; ***$p < 0.001$; ****$p < 0.0001$.

Abbreviations: OFT, Open Field Test; MWM, Morris Water Maze; RMWM, Reversal Morris Water Maze; NOL, Novel Object Location; NOR, Novel Object Recognition.

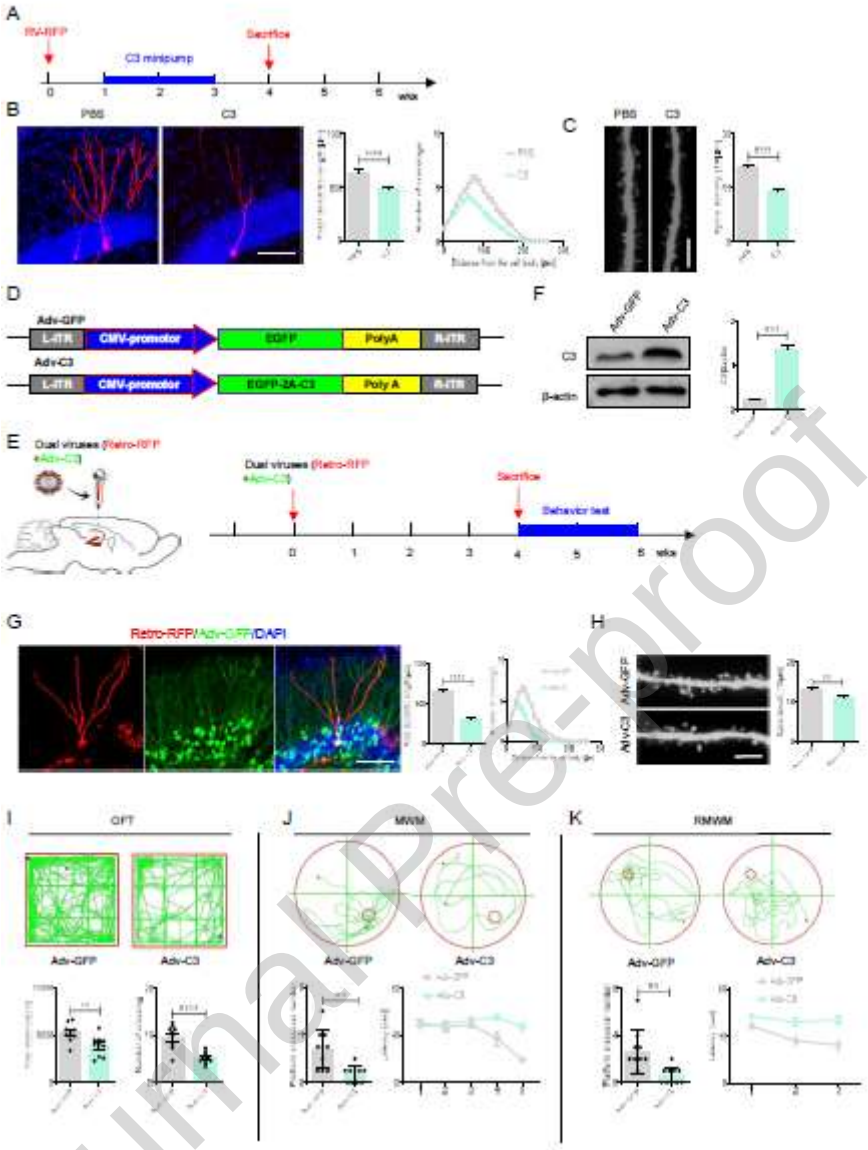

Fig. 3 The effects of C3 overexpression on hippocampal neuronal development and cognitive performance

(A) Timeline of the experiments to assay the development of hippocampal RFP^+ newborn neurons. 8-week-old wild-type mice received a stereotaxic injection of retroviruses and, one week later, received a mini-pump infusion of recombinant C3 protein or PBS into the hippocampal regions on both sides, with a total of 1 μg in 100 μL PBS on each side and at the rate of 0.25 μL per hour for 2 weeks.

(B) Representative confocal images and quantification of the dendritic length and dendritic complexity of RFP^+ newborn neurons in PBS or C3 mini-pump treated adult mice 1 week after retrovirus injection. Scale bars, 50 μm. n=30 neurons from 6 mice.

(C) Representative confocal images (left) and quantification (right) of dendritic spine density of retrovirally infected newborn neurons in mice injected with PBS or C3 mini-pump. Scale bar, 5 μm. n=30 neurons from 6 mice.

(D) Schematic diagram of the Adv-viral vectors for control (Adv-GFP) or C3 expression (Adv-

C3), with EGFP co-expression.

(E) Schematic diagram and timeline of the experiments for dual-virus (Retro-RFP and Adv-C3) injection and assays for cognitive performance in 8-week-old wild-type mice.

(F) C3 expression by immunoblotting of hippocampal lysates from control or C3-overexpressing mice. n=3 biological replicates per group.

(G) Representative confocal imaging and quantification of dendritic length and complexity of RFP^+ newborn neurons in adult mice receiving stereotactic injection of dual viruses (Retro-RFP and Adv-C3). Scale bars, 50 μm. n=30 neurons from 6 mice.

(H) Representative confocal images (left) and quantification (right) of dendritic spine density of retrovirally infected newborn neurons in mice injected with dual viruses. Scale bar, 5 μm. n=30 neurons from 6 mice.

(I) Mice stereotaxically injected with dual viruses (Retro-RFP and Adv-C3) underwent the standardized open field test before the Morris water maze (Fig. 3I) to evaluate their overall locomotor activities and low curiosity-like behaviours, with their representative movement paths and quantification of the open field test results by measuring the average total distance travelled and the average crossing numbers through the centre area shown here. n=10 animals per group.

(J) Representative movement paths of the mice receiving dual-virus (Retro-RFP and Adv-C3) stereotaxic injections in the standard Morris water maze (MWM) task. Quantification of the escape latencies to find the platform and the platform quadrant crossing numbers during the training sessions in the MWM task for both tested groups. n=10 animals per group.

(K) Representative reverse Morris water maze (RMWM) movement paths of the indicated groups. Quantification of RMWM escape latencies to find the platform and platform crossing numbers. n=10 animals per group.

Bar graphs are presented as means ± SEM; (B), (C), (F), (G) to (K), by Student's t-test. (B) and (G), dendritic complexity was evaluated with two-way ANOVA test. For (B), $p < 0.0001$. For (G), $p < 0.0001$. (J and K), by two-way ANOVA with Tukey's multiple comparisons. For (J), $p < 0.01$. For (K), $P < 0.01$. *$P < 0.05$, **$P < 0.01$, ***$P < 0.001$.

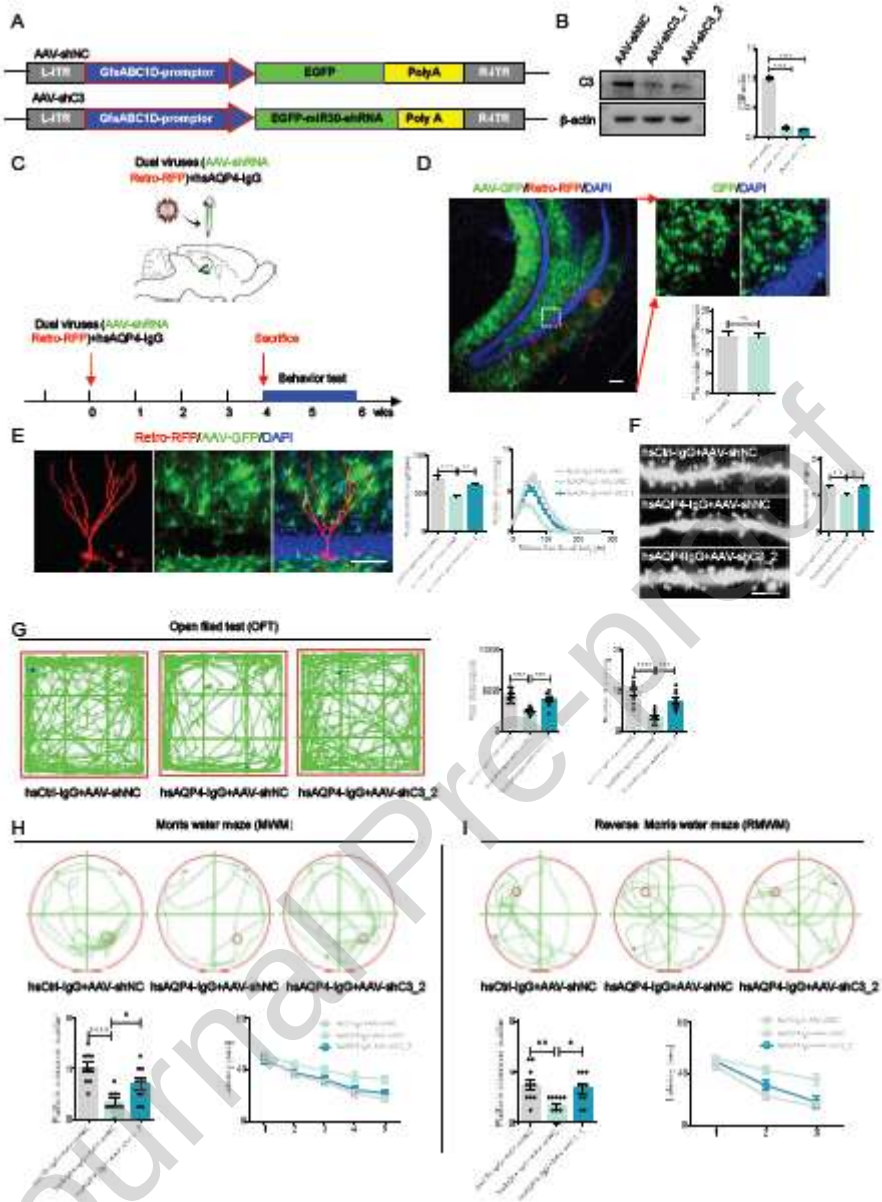

Fig. 4 The effect of C3 knockdown on hippocampal neuronal development and cognitive performance

(A) AAV-viral vectors to express three shRNAs for C3 knockdown (AAV-shC3_1, AAV-shC3_2) and a control shRNA (AAV-shNC).

(B) shRNA-mediated C3 knockdown efficiency. n=3 biological replicates per group.

(C) Schematic diagram and timeline of the experiments for dual-virus (AAV-shRNA and Retro-RFP) and hsAQP4-IgG mixture injection and analyses of RFP^+ newborn neurons.

(D) Representative confocal imaging and quantification of RFP^+ newborn neurons in adult mice receiving stereotactic injection of dual viruses (Retro-RFP and AAV-shRNA) and hsAQP4-IgG. Scale bars, 100 μm. n=10 hippocampal slices fron 10 mice.

(E) Representative confocal imaging and quantification of dendritic length and complexity of RFP^+ newborn neurons in adult mice receiving stereotactic injection of dual viruses (Retro-

RFP and AAV-shRNA) and hsAQP4-IgG. Scale bars, 50 μm. n=30 neurons from 10 mice.

(F) Representative confocal images (left) and quantification (right) of dendritic spine density of retrovirally infected newborn neurons in mice injected with dual viruses. Scale bar, 5 μm. n=30 neurons from 10 mice.

(G) The open field test (OFT) was performed before the MWM experiments to assess general locomotor activities and low curiosity-like behaviours. Representative movement paths and quantification of the open field test results are shown, measuring the average total distance travelled and the average crossing numbers through the centre area for the following groups: hsCtrl-IgG+AAV-shNC, hsAQP4-IgG+AAV-shNC, and hsAQP4-IgG+AAV-shC3_2. n=10 animals per group.

(H) Representative movement paths of the mice receiving mixed stereotactic injections in the standard Morris water maze (MWM) task. Quantification of the escape latencies to find the platform and the platform quadrant crossing numbers during the training sessions in the MWM task for the indicated groups. n=10 animals per group.

(I) Representative reverse Morris water maze (RMWM) movement paths of the indicated groups. Quantification of RMWM escape latencies to find the platform and platform crossing numbers. n=10 animals per group.

All quantitative data are presented as the mean ± SEM; For data in (D), the statistical significance was evaluated with Student's t-test for two-group comparisons; statistical analyses for results in (B), (E-I) were computed with one-way ANOVA and Tukey's post hoc multiple comparisons. For (E), dendritic complexity was evaluated with two-way ANOVA test. hsCtrl-IgG+AAV-shNC vs. hsAQP4-IgG+AAV-shNC, $p < 0.0001$; hsAQP4-IgG+AAV-shNC vs. hsAQP4-IgG+AAV-shC3_2, $p < 0.0001$. For (H) and (I), significance was evaluated with two-way ANOVA and Tukey's multiple-comparisons test. For (H), hsCtrl-IgG+AAV-shNC vs. hsAQP4-IgG+AAV-shNC, $p < 0.0001$; hsAQP4-IgG+AAV-shNC vs. hsAQP4-IgG+AAV-shC3_2, $p < 0.001$. For (I), hsCtrl-IgG+AAV-shNC vs. hsAQP4-IgG+AAV-shNC, $p < 0.0001$; hsAQP4-IgG+AAV-shNC vs. hsAQP4-IgG+AAV-shC3_2, $p < 0.001$. Nonsignificant comparisons were not identified. *$p < 0.05$; **$p < 0.01$; ***$p < 0.001$; ****$p < 0.0001$.

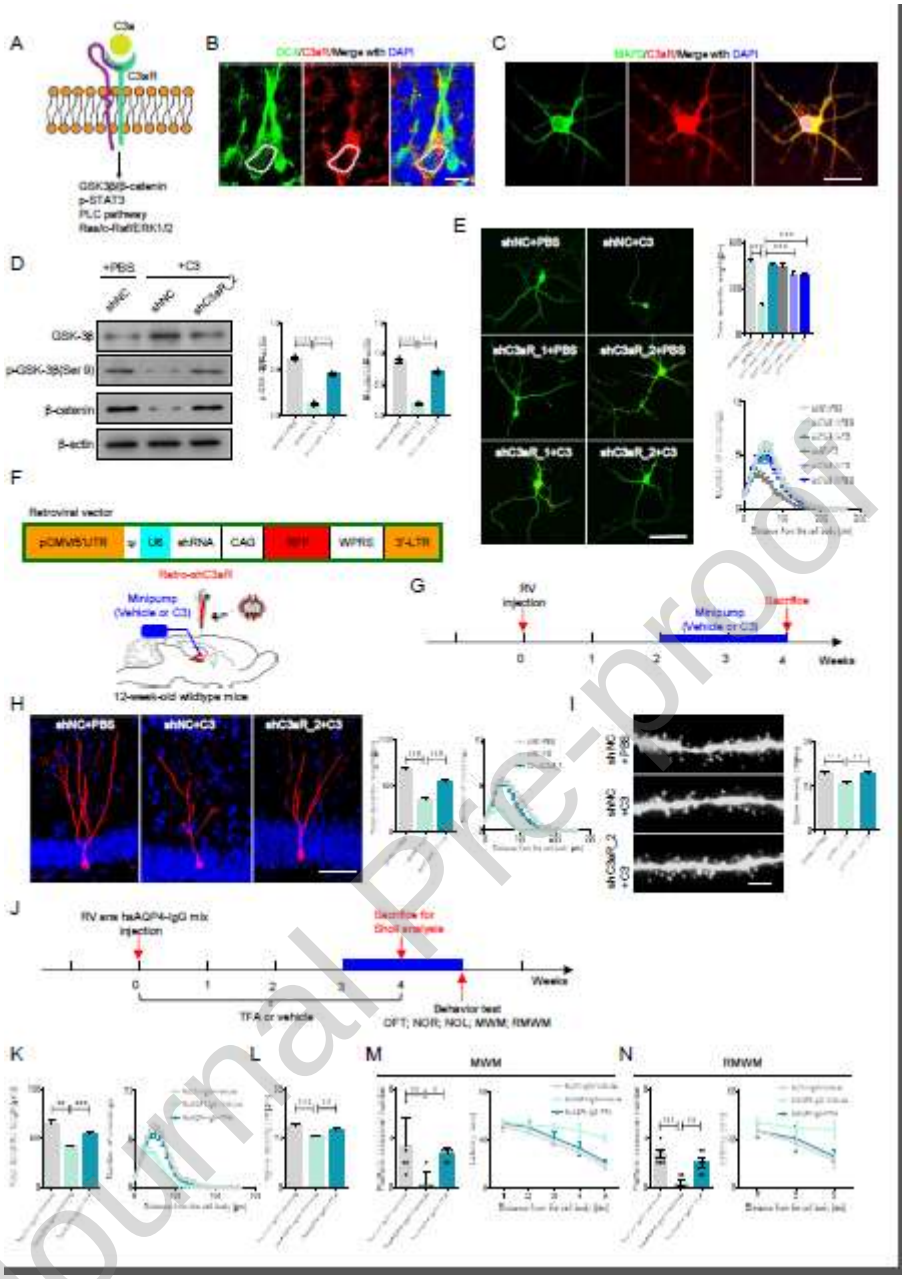

Fig. 5 The C3aR blockade effect on hippocampal neuronal development and cognitive performance affected by C3 or hsAQP4-IgG

(A) Summary of C3 receptors and downstream signalling pathways.

(B) Expression of C3aR receptor in immature (DCX^+) neurons in adult hippocampus. Scale bars, 10 μm.

(C) C3aR expression in cultured hippocampal primary neurons ($MAP2^+$). Scale bars, 50 μm.

(D) C3aR knockdown effect on GSK-3β/β-catenin pathway activation by C3 (100 ng/mL, 2-hour treatment). n=3 biological replicates per group.

(E) C3aR knockdown effect on primary hippocampal neuron development in shRNA-expressing cultures, with or without C3 for 3 days. Quantification of dendritic length (upper

panel) and dendritic complexity (lower panel) of primary hippocampal neurons in the indicated 6 groups by Sholl analysis. n=30 neurons from 3 independent experiments. Scale bars, 50 μm.

(F and G) Schematic diagram and timeline of the experiments for dual virus (Retro- shRNA and Retro-RFP) and C3 minipump injection.

(H) Representative confocal images and quantification of the dendritic length and dendritic complexity of RFP^+ newborn neurons treated with C3 minipump 2 weeks after retrovirus and shNC or shC3aR_2 injection. Scale bars, 50 μm. n=30 neurons from 6 mice.

(I) Representative confocal images (left) and quantification (right) of dendritic spine density of retrovirally infected newborn neurons in the indicated groups. Scale bar, 5 μm. n=30 neurons from 6 mice.

(J) Schematic diagram of in vivo assays for C3aR inhibitor trifluoroacetate (TFA, 1 mg/kg) efficacy to rescue hippocampal neuron development affected by hsAQP4-IgG–induced C3 signalling.

(K) Quantification of dendritic length and complexity of RFP^+ newborn neurons in adult mice receiving stereotactic injection of RV and hsAQP4-IgG and i.p. injection of trifluoroacetate (TFA, 1 mg/kg). Scale bars, 50 μm. n=30 neurons from 6 mice.

(L) Quantification of dendritic spine density of retrovirally infected newborn neurons in the indicated groups. n=30 neurons from 6 mice.

(M) Quantification of the escape latencies to find the platform and the platform quadrant crossing numbers during the training sessions in the MWM task for the indicated groups. n=6 animals per group.

(N) Quantification of RMWM escape latencies to find the platform and platform crossing numbers. n=6 animals per group.

All quantitative data are presented as the mean ± SEM; statistical analyses for results in (D), (E), (H), (I), and (K-N) were computed with one-way ANOVA and Tukey's post hoc multiple comparisons. For (E), (H) and (K), dendritic complexity was evaluated with two-way ANOVA test. For (E), shNC+PBS vs. shNC+C3, $p < 0.0001$; shNC+C3 vs. shC3aR_ 1+C3, $p < 0.0001$; shNC+C3 vs. shC3aR_2+C3, $p < 0.001$. For (H), shNC+PBS vs. shNC+C3, $p < 0.0001$; shNC+C3 vs. shC3aR_2+C3, $p<0.0001$. For (K), hsCtrl-IgG+Vehicle vs. hsAQP4-IgG+Vehicle, $p < 0.0001$; hsAQP4- IgG+Vehicle vs. hsAQP4-IgG+TFA, $p < 0.0001$. For (M) and (N), significance was evaluated with two-way ANOVA and Tukey's multiple-comparisons test. For (M), hsCtrl-IgG+Vehicle vs. hsAQP4-IgG+Vehicle, $p < 0.001$; hsAQP4-IgG+Vehicle vs. hsAQP4-IgG+TFA, $p < 0.01$. For (N), hsCtrl-IgG+Vehicle vs. hsAQP4-IgG+Vehicle, $p < 0.05$; hsAQP4-IgG+Vehicle vs. hsAQP4-IgG+TFA, $p < 0.05$. Nonsignificant comparisons were not identified. *$p < 0.05$; **$p < 0.01$; ***$p < 0.001$; ****$p < 0.0001$.

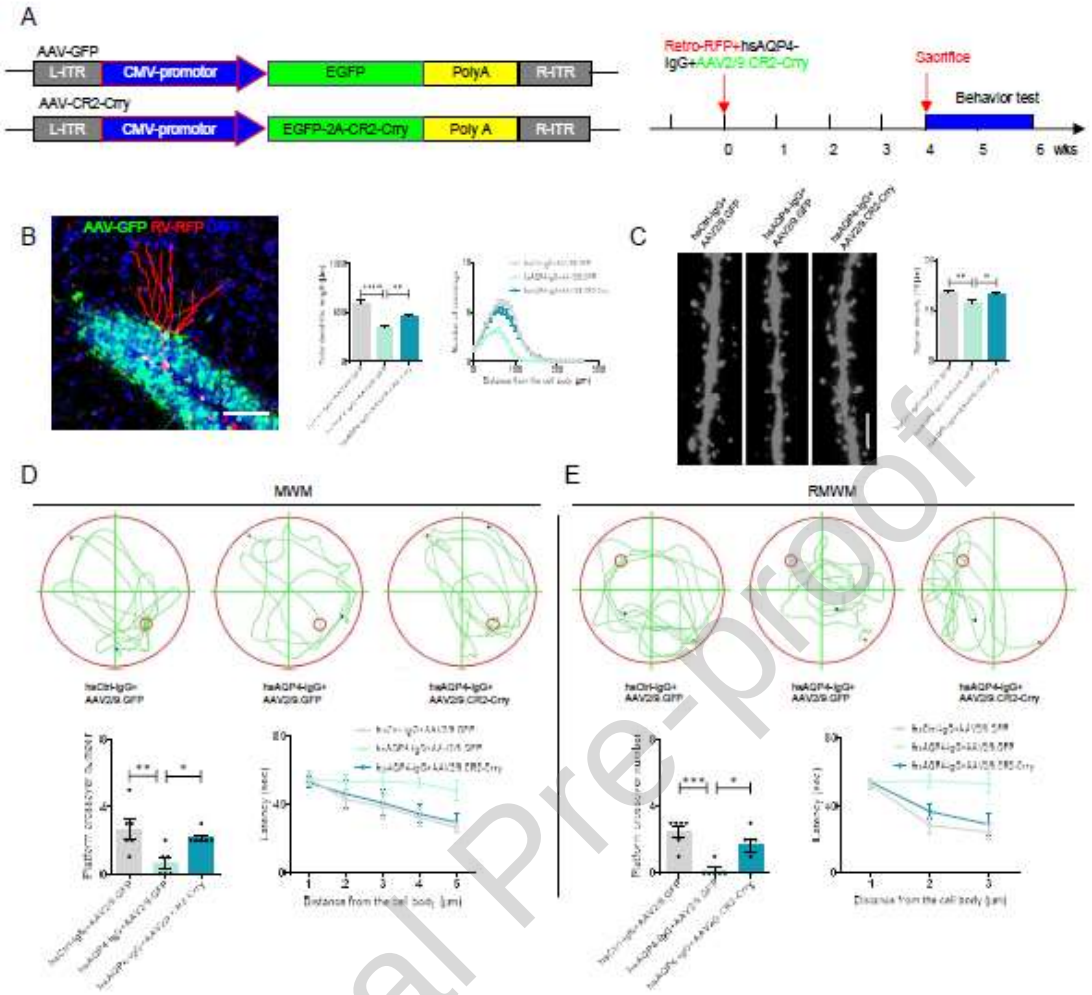

Fig. 6 The effects of AAV2/9.CR2-Crry gene therapy on neuronal development and behavioural performances

(A) Schematic diagram of AAV2/9.CR2-Crry construct and timeline of stereotaxic injection of Retro-RFP, hsAQP4-IgG, and AAV2/9.CR2-Crry.

(B) Representative confocal images and quantification of the dendritic length and dendritic complexity of RFP^+ newborn neurons in the indicated groups. Scale bars, 50 μm. n=30 neurons from 6 mice.

(C) Representative confocal images (left) and quantification (right) of dendritic spine density of retrovirally infected newborn neurons in the indicated groups. Scale bar, 5 μm. n=30 neurons from 6 mice.

(D) Representative movement paths of the mice receiving stereotaxic injections of Retro-RFP, hsAQP4-IgG, and AAV2/9.CR2-Crry in the standard MWM task. Quantification of the escape latencies to find the platform and the platform quadrant crossing numbers during the training sessions in the MWM task for the indicated groups. n=6 animals per group.

(E) Representative RMWM movement paths of the indicated groups. Quantification of

RMWM escape latencies to find the platform and platform crossing numbers. n=6 animals per group.

All quantitative data are presented as the mean ± SEM; statistical analyses for results in (B) to (E) were computed with one-way ANOVA and Tukey's post hoc multiple comparisons. For data in (B), dendritic complexity was evaluated with two-way ANOVA test; hsCtrl-IgG+AAV2/9. GFP vs. hsAQP4-IgG+AAV2/9.GFP, $p < 0.0001$; hsAQP4-IgG+AAV2/9.GFP vs. hsAQP4-IgG+AAV2/9.CR2-Crry, $p < 0.0001$. For data in (D) and (E), significance was evaluated with two-way ANOVA and Tukey's multiple-comparisons test. For (D), hsCtrl-IgG+AAV2/9.GFP vs. hsAQP4-IgG+AAV2/9.GFP, $p < 0.05$; hsAQP4-IgG+AAV2/9.GFP vs. hsAQP4-IgG+AAV2/9.CR2-Crry, $p < 0.05$. For (E), hsCtrl-IgG+AAV2/9.GFP vs. hsAQP4-IgG+AAV2/9.GFP, $p < 0.01$; hsAQP4-IgG+AAV2/9.GFP vs. hsAQP4-IgG+AAV2/9.CR2-Crry, $p < 0.05$. Nonsignificant comparisons were not identified. *$p < 0.05$; **$p < 0.01$; ***$p < 0.001$; ****$p < 0.0001$.

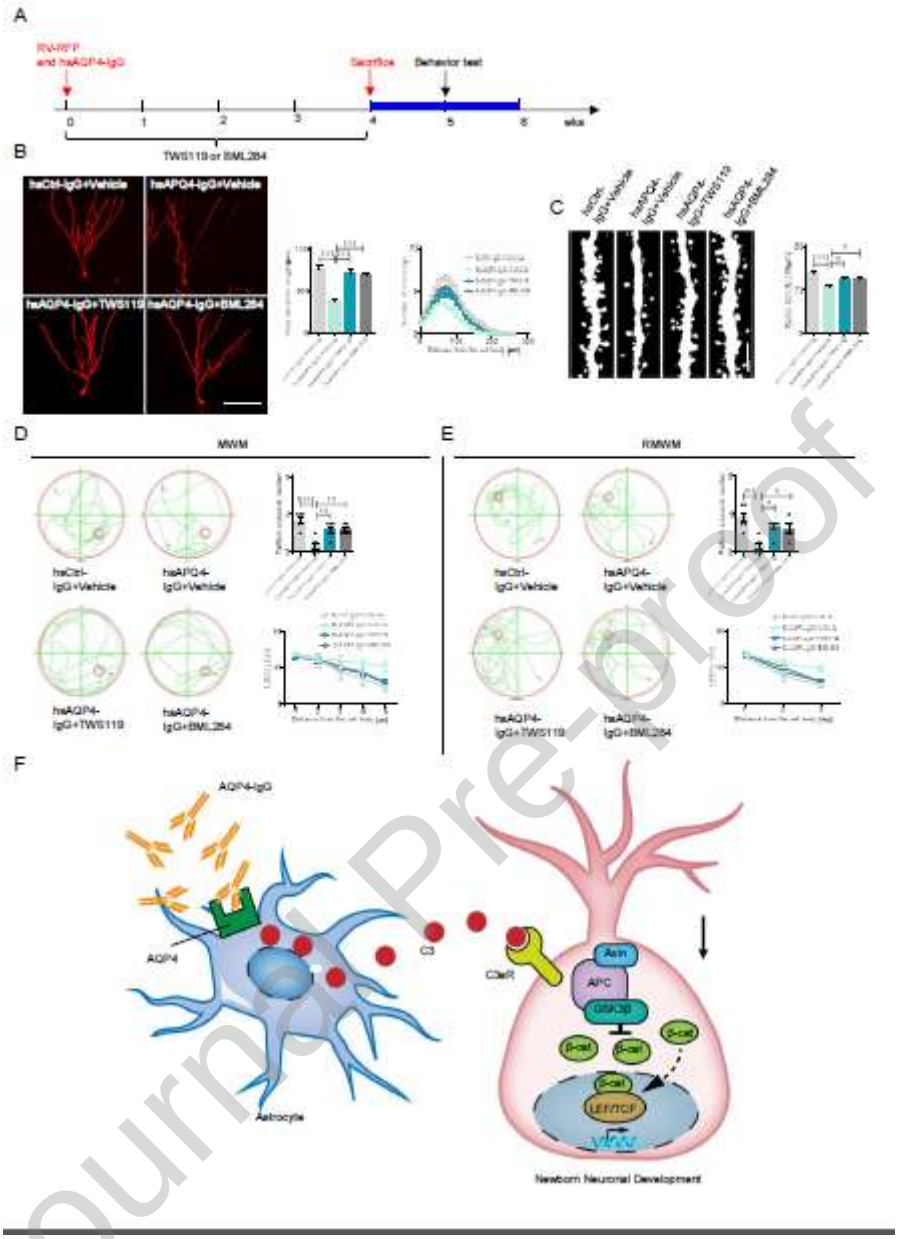

Fig. 7 The effects of regulation of GSK3β/β-Catenin signalling on hippocampal neuronal development and cognitive performance

(A) Timeline for assays of hippocampal neuron development in RV-RFP and hsAQP4- IgG–injected mice, receiving a potent GSK-3β inhibitor, TWS119 (30 mg/kg), and an agonistic β-catenin inhibitor, BML284 (4 mg/kg), intraperitoneally daily for 4 weeks.

(B) Representative confocal images and quantification of the dendritic length and dendritic complexity of RFP^+ newborn neurons in the indicated groups. Scale bars, 50 μm. n=30 neurons from 6 mice.

(C) Representative confocal images (left) and quantification (right) of dendritic spine density of retrovirally infected newborn neurons in the indicated groups. Scale bar, 5 μm. n=30 neurons from 6 mice.

(D) Representative movement paths of the mice in the MWM task. Quantification of the escape latencies to find the platform and the platform quadrant crossing numbers during the training sessions in the MWM task for the indicated groups. n=6 animals per group.

(E) Representative RMWM movement paths of the indicated groups. Quantification of RMWM escape latencies to find the platform and platform crossing numbers. n=6 animals per group.

(F) Model of AQP4-IgG-treated astrocytes inhibiting newborn neuron development through secretion of C3 into the neurogenic niche in the adult hippocampus.

All quantitative data are presented as the mean ± SEM; for data in (B) to (E), statistical significance was evaluated with one-way ANOVA and Tukey's post hoc multiple comparisons. For data in (B), dendritic complexity was evaluated with two-way ANOVA test; hsCtrl-IgG+Vehicle vs. hsAQP4-IgG+Vehicle, $p< 0.0001$; hsAQP4-IgG+Vehicle vs. hsAQP4-IgG+TWS119, $p<0.01$; hsAQP4-IgG+Vehicle vs. hsAQP4-IgG+BML284, $p<0.001$. For (D) and (E), significance was evaluated with two-way ANOVA and Tukey's multiple-comparisons test. For (D), hsCtrl-IgG+Vehicle vs. hsAQP4-IgG+Vehicle, $p < 0.01$; hsAQP4-IgG+Vehicle vs. hsAQP4- IgG+TWS119, $p < 0.05$; hsAQP4-IgG+Vehicle vs. hsAQP4-IgG+BML284, $p < 0.05$. For (E), hsCtrl-IgG+Vehicle vs. hsAQP4-IgG+Vehicle, $p < 0.001$; hsAQP4-IgG+Vehicle vs. hsAQP4-IgG+TWS119, $p < 0.01$; hsAQP4-IgG+Vehicle vs. hsAQP4-IgG+BML284, $p < 0.01$. Nonsignificant comparisons were not identified. *$p < 0.05$; **$p < 0.01$; ***$p < 0.001$; ****$p < 0.0001$.

References

Abboud, H., Salazar-Camelo, A., George, N., Planchon, S.M., Matiello, M., Mealy, M.A., Goodman, A., On-behalf of the Guthy-Jackson Foundation, N.M.O.I.C.C., 2022. Symptomatic and restorative therapies in neuromyelitis optica spectrum disorders. *J Neurol* 269**,** 1786-1801.

Alawieh, A., Elvington, A., Zhu, H., Yu, J., Kindy, M.S., Atkinson, C., Tomlinson, S., 2015. Modulation of post-stroke degenerative and regenerative processes and subacute protection by site-targeted inhibition of the alternative pathway of complement. *Journal of neuroinflammation* 12**,** 247.

Alawieh, A., Langley, E.F., Weber, S., Adkins, D., Tomlinson, S., 2018. Identifying the Role of Complement in Triggering Neuroinflammation after Traumatic Brain Injury. *The Journal of neuroscience : the official journal of the Society for Neuroscience* 38**,** 2519-2532.

Ames, R.S., Lee, D., Foley, J.J., Jurewicz, A.J., Tornetta, M.A., Bautsch, W., Settmacher, B., Klos, A., Erhard, K.F., Cousins, R.D., Sulpizio, A.C., Hieble, J.P., McCafferty, G., Ward, K.W., Adams, J.L., Bondinell, W.E., Underwood, D.C., Osborn, R.R., Badger, A.M., Sarau, H.M., 2001. Identification of a selective nonpeptide antagonist of the anaphylatoxin C3a receptor that demonstrates antiinflammatory activity in animal models. *J Immunol* 166**,** 6341-6348.

Asavapanumas, N., Tradtrantip, L., Verkman, A.S., 2021. Targeting the complement system in neuromyelitis optica spectrum disorder. *Expert opinion on biological therapy* 21**,** 1073-1086.

Atkinson, C., Song, H., Lu, B., Qiao, F., Burns, T.A., Holers, V.M., Tsokos, G.C., Tomlinson, S., 2005. Targeted complement inhibition by C3d recognition ameliorates tissue injury without apparent increase in susceptibility to infection. *J Clin Invest* 115**,** 2444-2453.

Barker, G.R., Warburton, E.C., 2011. When is the hippocampus involved in recognition memory? *The Journal of neuroscience : the official journal of the Society for Neuroscience* 31**,** 10721-10731.

Bourel, J., Planche, V., Dubourdieu, N., Oliveira, A., Sere, A., Ducourneau, E.G., Tible, M., Maitre, M., Leste-Lasserre, T., Nadjar, A., Desmedt, A., Ciofi, P., Oliet, S.H., Panatier, A., Tourdias, T., 2021. Complement C3 mediates early hippocampal neurodegeneration and memory impairment in experimental multiple sclerosis. *Neurobiol Dis* 160**,** 105533.

Cacciaguerra, L., Valsasina, P., Meani, A., Riccitelli, G.C., Radaelli, M., Rocca, M.A., Filippi, M., 2021. Volume of hippocampal subfields and cognitive deficits in neuromyelitis optica spectrum disorders. *Eur J Neurol* 28**,** 4167-4177.

Carpanini, S.M., Torvell, M., Morgan, B.P., 2019. Therapeutic Inhibition of the Complement System in Diseases of the Central Nervous System. *Frontiers in immunology* 10**,** 362.

Chen, J.F., Liu, K., Hu, B., Li, R.R., Xin, W., Chen, H., Wang, F., Chen, L., Li, R.X., Ren, S.Y., Xiao, L., Chan, J.R., Mei, F., 2021. Enhancing myelin renewal reverses cognitive dysfunction in a murine model of Alzheimer's disease. *Neuron* 109**,** 2292-2307.e2295.

Chen, T., Lennon, V.A., Liu, Y.U., Bosco, D.B., Li, Y., Yi, M.H., Zhu, J., Wei, S., Wu, L.J., 2020. Astrocyte-microglia interaction drives evolving neuromyelitis optica lesion. *J Clin Invest* 130**,** 4025-4038.

Chenn, A., Walsh, C.A., 2002. Regulation of cerebral cortical size by control of cell cycle exit in neural precursors. *Science (New York, N.Y.)* 297**,** 365-369.

Cope, E.C., Gould, E., 2019. Adult Neurogenesis, Glia, and the Extracellular Matrix. *Cell stem*

cell 24**,** 690-705.

Czarnecka, D., Oset, M., Karlińska, I., Stasiołek, M., 2020. Cognitive impairment in NMOSD-More questions than answers. *Brain and behavior* 10**,** e01842.

Davoust, N., Jones, J., Stahel, P.F., Ames, R.S., Barnum, S.R., 1999. Receptor for the C3a anaphylatoxin is expressed by neurons and glial cells. *Glia* 26**,** 201-211.

Denoth-Lippuner, A., Jessberger, S., 2021. Formation and integration of new neurons in the adult hippocampus. *Nature Reviews Neuroscience* 22**,** 223-236.

Gonçalves, J.T., Schafer, S.T., Gage, F.H., 2016. Adult Neurogenesis in the Hippocampus: From Stem Cells to Behavior. *Cell* 167**,** 897-914.

Herrera, A., Menendez, A., Ochoa, A., Bardia, L., Colombelli, J., Pons, S., 2023. Neurogenesis redirects β-catenin from adherens junctions to the nucleus to promote axonal growth. *Development (Cambridge, England)* 150.

Hirabayashi, Y., Itoh, Y., Tabata, H., Nakajima, K., Akiyama, T., Masuyama, N., Gotoh, Y., 2004. The Wnt/beta-catenin pathway directs neuronal differentiation of cortical neural precursor cells. *Development (Cambridge, England)* 131**,** 2791-2801.

Holers, V.M., 2014. Complement and its receptors: new insights into human disease. *Annu Rev Immunol* 32**,** 433-459.

Hu, X., Tomlinson, S., Barnum, S.R., 2012. Targeted inhibition of complement using complement receptor 2-conjugated inhibitors attenuates EAE. *Neuroscience letters* 531**,** 35-39.

Huang, Y.A., Zhou, B., Nabet, A.M., Wernig, M., Sudhof, T.C., 2019. Differential Signaling Mediated by ApoE2, ApoE3, and ApoE4 in Human Neurons Parallels Alzheimer's Disease Risk. *The Journal of neuroscience : the official journal of the Society for Neuroscience* 39**,** 7408-7427.

Huang, Y.A., Zhou, B., Wernig, M., Sudhof, T.C., 2017. ApoE2, ApoE3, and ApoE4 Differentially Stimulate APP Transcription and Abeta Secretion. *Cell* 168**,** 427-441 e421.

Humbles, A.A., Lu, B., Nilsson, C.A., Lilly, C., Israel, E., Fujiwara, Y., Gerard, N.P., Gerard, C., 2000. A role for the C3a anaphylatoxin receptor in the effector phase of asthma. *Nature* 406**,** 998-1001.

Jiang, W., Zhu, F., Xu, H., Xu, L., Li, H., Yang, X., Khan Afridi, S., Lai, S., Qiu, X., Liu, C., Li, H., Long, Y., Wang, Y., Connolly, K., Elias, J.A., Lee, C.G., Cui, Y., Huang, Y.A., Qiu, W., Tang, C., 2023. CHI3L1 signaling impairs hippocampal neurogenesis and cognitive function in autoimmune-mediated neuroinflammation. *Sci Adv* 9**,** eadg8148.

Lennon, V.A., Wingerchuk, D.M., Kryzer, T.J., Pittock, S.J., Lucchinetti, C.F., Fujihara, K., Nakashima, I., Weinshenker, B.G., 2004. A serum autoantibody marker of neuromyelitis optica: distinction from multiple sclerosis. *Lancet (London, England)* 364**,** 2106-2112.

Li, Q., Zhao, Y., Guo, H., Li, Q., Yan, C., Li, Y., He, S., Wang, N., Wang, Q., 2023. Impaired lipophagy induced-microglial lipid droplets accumulation contributes to the buildup of TREM1 in diabetes-associated cognitive impairment. *Autophagy* 19**,** 2639-2656.

Lian, H., Litvinchuk, A., Chiang, A.C., Aithmitti, N., Jankowsky, J.L., Zheng, H., 2016. Astrocyte-Microglia Cross Talk through Complement Activation Modulates Amyloid Pathology in Mouse Models of Alzheimer's Disease. *The Journal of neuroscience : the official journal of the Society for Neuroscience* 36**,** 577-589.

Lian, H., Yang, L., Cole, A., Sun, L., Chiang, A.C., Fowler, S.W., Shim, D.J., Rodriguez-Rivera, J., Taglialatela, G., Jankowsky, J.L., Lu, H.C., Zheng, H., 2015a. NFkappaB-activated astroglial release of complement C3 compromises neuronal morphology and function associated with Alzheimer's disease. *Neuron* 85**,** 101-115.

Lian, H., Yang, L., Cole, A., Sun, L., Chiang, A.C., Fowler, S.W., Shim, D.J., Rodriguez-Rivera, J., Taglialatela, G., Jankowsky, J.L., Lu, H.C., Zheng, H., 2015b. NFκB-activated astroglial release of complement C3 compromises neuronal morphology and function associated with Alzheimer's disease. *Neuron* 85**,** 101-115.

Lie, D.C., Colamarino, S.A., Song, H.J., Désiré, L., Mira, H., Consiglio, A., Lein, E.S., Jessberger, S., Lansford, H., Dearie, A.R., Gage, F.H., 2005. Wnt signalling regulates adult hippocampal neurogenesis. *Nature* 437**,** 1370-1375.

Litvinchuk, A., Wan, Y.W., Swartzlander, D.B., Chen, F., Cole, A., Propson, N.E., Wang, Q., Zhang, B., Liu, Z., Zheng, H., 2018. Complement C3aR Inactivation Attenuates Tau Pathology and Reverses an Immune Network Deregulated in Tauopathy Models and Alzheimer's Disease. *Neuron* 100**,** 1337-1353 e1335.

Liu, Y., Fu, Y., Schoonheim, M.M., Zhang, N., Fan, M., Su, L., Shen, Y., Yan, Y., Yang, L., Wang, Q., Zhang, N., Yu, C., Barkhof, F., Shi, F.D., 2015. Structural MRI substrates of cognitive impairment in neuromyelitis optica. *Neurology* 85**,** 1491-1499.

Llorens-Martín, M., Rábano, A., Ávila, J., 2015. The Ever-Changing Morphology of Hippocampal Granule Neurons in Physiology and Pathology. *Frontiers in neuroscience* 9**,** 526.

Lopez-Soley, E., Meca-Lallana, J.E., Llufriu, S., Blanco, Y., Gómez-Ballesteros, R., Maurino, J., Pérez-Miralles, F., Forero, L., Calles, C., Martinez-Gines, M.L., Gonzalez-Suarez, I., Boyero, S., Romero-Pinel, L., Sempere Á, P., Meca-Lallana, V., Querol, L., Costa-Frossard, L., Sepulveda, M., Solana, E., 2022. Cognitive Performance and Health-Related Quality of Life in Patients with Neuromyelitis Optica Spectrum Disorder. *Journal of personalized medicine* 12.

López de Victoria, A., Gorham, R.D., Jr., Bellows-Peterson, M.L., Ling, J., Lo, D.D., Floudas, C.A., Morikis, D., 2011. A new generation of potent complement inhibitors of the Compstatin family. *Chemical biology & drug design* 77**,** 431-440.

Ma, X., Kermode, A.G., Hu, X., Qiu, W., 2020. NMOSD acute attack: Understanding, treatment and innovative treatment prospect. *J Neuroimmunol* 348**,** 577387.

Mastellos, D.C., Hajishengallis, G., Lambris, J.D., 2023. A guide to complement biology, pathology and therapeutic opportunity. *Nature Reviews Immunology*.

Mastellos, D.C., Ricklin, D., Lambris, J.D., 2019. Clinical promise of next-generation complement therapeutics. *Nature reviews. Drug discovery* 18**,** 707-729.

Matsumoto, J., Uehara, T., Urakawa, S., Takamura, Y., Sumiyoshi, T., Suzuki, M., Ono, T., Nishijo, H., 2014. 3D video analysis of the novel object recognition test in rats. *Behavioural brain research* 272**,** 16-24.

Minton, K., 2014. Innate immunity: The inside story on complement activation. *Nat Rev Immunol* 14**,** 61.

Murase, S., Mosser, E., Schuman, E.M., 2002. Depolarization drives beta-Catenin into neuronal spines promoting changes in synaptic structure and function. *Neuron* 35**,** 91-105.

Nytrova, P., Potlukova, E., Kemlink, D., Woodhall, M., Horakova, D., Waters, P., Havrdova, E., Zivorova, D., Vincent, A., Trendelenburg, M., 2014. Complement activation in patients with

neuromyelitis optica. *J Neuroimmunol* 274**,** 185-191.

Pittock, S.J., Berthele, A., Fujihara, K., Kim, H.J., Levy, M., Palace, J., Nakashima, I., Terzi, M., Totolyan, N., Viswanathan, S., Wang, K.-C., Pace, A., Fujita, K.P., Armstrong, R., Wingerchuk, D.M., 2019. Eculizumab in Aquaporin-4–Positive Neuromyelitis Optica Spectrum Disorder. 381**,** 614-625.

Pozo-Rodrigálvarez, A., Ollaranta, R., Skoog, J., Pekny, M., Pekna, M., 2021. Hyperactive Behavior and Altered Brain Morphology in Adult Complement C3a Receptor Deficient Mice. *Frontiers in immunology* 12**,** 604812.

Price, J., Turner, D., Cepko, C., 1987. Lineage analysis in the vertebrate nervous system by retrovirus-mediated gene transfer. *Proc Natl Acad Sci U S A* 84**,** 156-160.

Reid, R.C., Yau, M.K., Singh, R., Hamidon, J.K., Lim, J., Stoermer, M.J., Fairlie, D.P., 2014. Potent heterocyclic ligands for human complement c3a receptor. *J Med Chem* 57**,** 8459-8470.

Reis, E.S., Mastellos, D.C., Hajishengallis, G., Lambris, J.D., 2019. New insights into the immune functions of complement. *Nat Rev Immunol* 19**,** 503-516.

Ricklin, D., Lambris, J.D., 2013. Complement in immune and inflammatory disorders: pathophysiological mechanisms. *J Immunol* 190**,** 3831-3838.

Ricklin, D., Reis, E.S., Lambris, J.D., 2016. Complement in disease: a defence system turning offensive. *Nat Rev Nephrol* 12**,** 383-401.

Shi, Q., Chowdhury, S., Ma, R., Le, K.X., Hong, S., Caldarone, B.J., Stevens, B., Lemere, C.A., 2017. Complement C3 deficiency protects against neurodegeneration in aged plaque-rich APP/PS1 mice. *Sci Transl Med* 9.

Stellwagen, D., Malenka, R.C., 2006. Synaptic scaling mediated by glial TNF-alpha. *Nature* 440**,** 1054-1059.

Stephan, A.H., Barres, B.A., Stevens, B., 2012. The complement system: an unexpected role in synaptic pruning during development and disease. *Annual review of neuroscience* 35**,** 369-389.

Sun, B., Halabisky, B., Zhou, Y., Palop, J.J., Yu, G., Mucke, L., Gan, L., 2009. Imbalance between GABAergic and Glutamatergic Transmission Impairs Adult Neurogenesis in an Animal Model of Alzheimer's Disease. *Cell stem cell* 5**,** 624-633.

Tang, C., Guo, W., 2021. Implantation of a mini-osmotic pump plus stereotactical injection of retrovirus to study newborn neuron development in adult mouse hippocampus. *STAR protocols* 2**,** 100374.

Trinchero, M.F., Buttner, K.A., Sulkes Cuevas, J.N., Temprana, S.G., Fontanet, P.A., Monzón-Salinas, M.C., Ledda, F., Paratcha, G., Schinder, A.F., 2017. High Plasticity of New Granule Cells in the Aging Hippocampus. *Cell Rep* 21**,** 1129-1139.

Vignesh, P., Rawat, A., Sharma, M., Singh, S., 2017. Complement in autoimmune diseases. *Clin Chim Acta* 465**,** 123-130.

Vorhees, C.V., Williams, M.T., 2006. Morris water maze: procedures for assessing spatial and related forms of learning and memory. *Nature Protocols* 1**,** 848-858.

Walker-Caulfield, M.E., Guo, Y., Johnson, R.K., McCarthy, C.B., Fitz-Gibbon, P.D., Lucchinetti, C.F., Howe, C.L., 2015. NFκB signaling drives pro-granulocytic astroglial responses to neuromyelitis optica patient IgG. *Journal of neuroinflammation* 12**,** 185.

Wei, Y., Chen, T., Bosco, D.B., Xie, M., Zheng, J., Dheer, A., Ying, Y., Wu, Q., Lennon, V.A., Wu, L.J., 2021. The complement C3-C3aR pathway mediates microglia-astrocyte interaction following status epilepticus. *Glia* 69**,** 1155-1169.

Wu, T., Dejanovic, B., Gandham, V.D., Gogineni, A., Edmonds, R., Schauer, S., Srinivasan, K., Huntley, M.A., Wang, Y., Wang, T.M., Hedehus, M., Barck, K.H., Stark, M., Ngu, H., Foreman, O., Meilandt, W.J., Elstrott, J., Chang, M.C., Hansen, D.V., Carano, R.A.D., Sheng, M., Hanson, J.E., 2019. Complement C3 Is Activated in Human AD Brain and Is Required for Neurodegeneration in Mouse Models of Amyloidosis and Tauopathy. *Cell Rep* 28**,** 2111-2123 e2116.

Xu, L., Xu, H., Chen, S., Jiang, W., Afridi, S.K., Wang, Y., Ren, X., Zhao, Y., Lai, S., Qiu, X., Alvin Huang, Y.W., Cui, Y., Yang, H., Qiu, W., Tang, C., 2023. Inhibition of complement C3 signaling ameliorates locomotor and visual dysfunction in autoimmune inflammatory diseases. *Mol Ther* 31**,** 2715-2733.

Yick, L.W., Tang, C.H., Ma, O.K., Kwan, J.S., Chan, K.H., 2020. Memantine ameliorates motor impairments and pathologies in a mouse model of neuromyelitis optica spectrum disorders. *J Neuroinflammation* 17**,** 236.

Zakani, M., Nigritinou, M., Ponleitner, M., Takai, Y., Hofmann, D., Hillebrand, S., Höftberger, R., Bauer, J., Lasztoczi, B., Misu, T., Kasprian, G., Rommer, P., Bradl, M., 2023. Paths to hippocampal damage in neuromyelitis optica spectrum disorders. *Neuropathology and applied neurobiology* 49**,** e12893.

Zhang, H., Kim, Y., Ro, E.J., Ho, C., Lee, D., Trapp, B.D., Suh, H., 2020. Hippocampal Neurogenesis and Neural Circuit Formation in a Cuprizone-Induced Multiple Sclerosis Mouse Model. *The Journal of neuroscience : the official journal of the Society for Neuroscience* 40**,** 447-458.

Zhang, Y., Chen, K., Sloan, S.A., Bennett, M.L., Scholze, A.R., O'Keeffe, S., Phatnani, H.P., Guarnieri, P., Caneda, C., Ruderisch, N., Deng, S., Liddelow, S.A., Zhang, C., Daneman, R., Maniatis, T., Barres, B.A., Wu, J.Q., 2014. An RNA-sequencing transcriptome and splicing database of glia, neurons, and vascular cells of the cerebral cortex. *J Neurosci* 34**,** 11929-11947.

Declaration of Interests

The authors declare no competing interests.

Highlights:

- Astrocyte-secreted C3 impairs hippocampal neuronal development
- Knockdown of C3 in astrocyte improves neuronal development deficits and cognition
- C3 engages with C3aR to inhibits neuronal development

- Reactivation of β-catenin signaling ameliorates neuronal development and cognition